

FULLY-HEAVY TETRAQUARK SPECTROSCOPY IN THE RELATIVISTIC QUARK MODEL

Rudolf N. Faustov¹, Vladimir O. Galkin¹ and Elena M. Savchenko^{1,2,*}

¹ Federal Research Center “Computer Science and Control”, Russian Academy of Sciences, Vavilov Street 40, 119333 Moscow, Russia

² Faculty of Physics, M.V.Lomonosov Moscow State University, Leninskie Gory 1-2, 119991 Moscow, Russia

* Correspondence: savchenko.em16@physics.msu.ru

Abstract: Masses of the ground and excited (1P, 2S, 1D, 2P, 3S) states of the fully-heavy tetraquarks, composed of charm (c) and bottom (b) quarks and antiquarks, are calculated in the diquark-antidiquark picture within the relativistic quark model based on the quasipotential approach and quantum chromodynamics. The quasipotentials of the quark-quark and diquark-antidiquark interactions are constructed similarly to the previous consideration of mesons and baryons. Relativistic effects are consistently taken into account. A tetraquark is considered as a bound state of a diquark and an antidiquark. The finite size of the diquark is taken into account, using the form factors of the diquark-gluon interaction. It is shown that most of the investigated states of tetraquarks lie above the decay thresholds into a meson pair, as a result they can be observed only as broad resonances. The narrow state $X(6900)$ recently discovered in the $di-J/\psi$ production spectrum by the LHCb, CMS and ATLAS Collaborations corresponds to an excited state of the fully-charmed tetraquark. Other recently discovered exotic heavy resonances $X(6200)$, $X(6400)$, $X(6600)$, $X(7200)$, $X(7300)$ can also be interpreted as the different excitations of the fully-charmed tetraquark.

Keywords: tetraquark spectroscopy, diquark, heavy quarks, relativistic quark model

1. Introduction

The quark model of hadrons predicts various possible stable combinations of valence quarks and antiquarks, but for many decades only two kinds of combinations were observed: baryons, consisting of three quarks (qqq), and mesons, consisting of a quark and an antiquark ($q\bar{q}$). Other possible combinations such as tetraquarks ($qq\bar{q}\bar{q}$), pentaquarks ($qqqq\bar{q}$), glueballs (gg), hybrids ($q\bar{q}g$) and others were called “exotic”.

For many years the very existence of those states was unclear, since there was no convincing experimental evidence for them. The first reliable candidate for an exotic state was the $X(3872)$ particle (Belle 2003 [1]). This is a charmonium-like state with an extremely narrow width ($\Gamma = 1.19 \pm 0.21$ MeV [2]) and uncharacteristic decays breaking the isospin ($\frac{Br(X(3872) \rightarrow \omega J/\psi)}{Br(X(3872) \rightarrow \pi^+ \pi^- J/\psi)} = 1.1 \pm 0.4$ [1,3]). Thus, the $X(3872)$ does not fit into the naive quark picture of hadrons except as in the form of the two-quark–two-antiquark state ($cu\bar{c}\bar{u}$). Soon after, the first explicitly exotic state $Z_c^\pm(4430)$ (LHCb 2014 [4]) was discovered. This particle is of special interest since it is the charged charmonium state. A nonzero electric charge means that, in addition to a pair of charmed quark and antiquark, it contains also a light quark and antiquark of different flavors ($cu\bar{c}\bar{d}$, $cd\bar{c}\bar{u}$). Currently a few dozen of candidates and reliably confirmed tetraquarks ($cc\bar{c}\bar{c} - X(6900) - \text{LHCb 2020 [5], CMS 2022 [6], ATLAS 2022 [7], etc.}$) and pentaquarks ($uudc\bar{c} - P_c^+(4380), P_c^+(4450) - \text{LHCb 2015 [8]}$) have been discovered. The most recent detailed review can be found in Ref. [9].

The unified theoretical picture of exotic states has not been developed yet. In the absence of a direct description of hadrons from first principles of QCD, theorists have to use model assumptions about the structure and nature of the interaction of quarks in exotic hadrons. As a result, there are theoretical approaches that assume a different composition of exotic states and methods for their nonperturbative description. The predictions obtained within their framework agree with experimental data with varying degrees of



Citation: Faustov, R.N.; Galkin, V.O.; Savchenko, E.M. *Preprints* **2022**, *1*, 0. <https://doi.org/>

Publisher’s Note: MDPI stays neutral with regard to jurisdictional claims in published maps and institutional affiliations.



Copyright: © 2022 by the authors. Licensee MDPI, Basel, Switzerland. This article is an open access article distributed under the terms and conditions of the Creative Commons Attribution (CC BY) license (<https://creativecommons.org/licenses/by/4.0/>).

success. The object of our research from all exotic states are fully-heavy tetraquarks, consisting of two heavy quarks and two heavy antiquarks. This choice significantly reduces the number of approaches applicable for their description. At the moment, there are already a number of theoretical calculations within the framework of different models, but there is no consensus on which of the predicted states are long-living enough for their experimental detection.

Experimental searches for such states are actively conducted at Large Hadron Collider (LHC) in CERN. At present, the LHCb [5,10], CMS [6,11,12] and ATLAS [7] Collaborations are actively searching for the fully-charmed $cc\bar{c}\bar{c}$ and fully-bottom $bb\bar{b}\bar{b}$ tetraquarks. The fully-charmed states $cc\bar{c}\bar{c}$ are searched as the intermediate resonances in the processes $p + p \rightarrow J/\psi(1S)J/\psi(1S)$, $p + p \rightarrow J/\psi(1S)\psi(2S)$ and $p + p \rightarrow J/\psi\mu^+\mu^-$ at $\sqrt{s} = 7, 8$ and 13 TeV (LHCb). The predicted mass of the $cc\bar{c}\bar{c}$ tetraquark lies in the range of 5.8 – 7.4 GeV. Searches for it were performed in the mass range 6.2 – 7.4 GeV. In 2020 the LHCb Collaboration announced the discovery of the narrow resonance $X(6900)$ in di- J/ψ spectrum [5], which, according to the measured mass and width, is a candidate for the excited $cc\bar{c}\bar{c}$ state. Also several other broad structures peaking at about 6.4 and 7.2 GeV were reported. They can be other excitations of the same $cc\bar{c}\bar{c}$ tetraquark. Later in 2022 CMS [6] and ATLAS [7] Collaborations presented preliminary data confirming $X(6900)$ and giving hints of a few more states including structures at 6.4 and 7.2 GeV.

In the sector of fully-bottom tetraquarks $bb\bar{b}\bar{b}$ there is no progress yet. These tetraquark states are searched as the intermediate resonances in the processes $p + p \rightarrow Y(1S)Y(1S)$ and $p + p \rightarrow Y\mu^+\mu^-$ at $\sqrt{s} = 7, 8$ and 13 TeV (LHCb) and 8 and 13 TeV (CMS). The predicted mass of the $bb\bar{b}\bar{b}$ state lies in the range of 18.4 – 18.8 GeV. Searches for the $bb\bar{b}\bar{b}$ state were carried out in the mass range of 17.5 – 20.0 GeV (LHCb) and 17.5 – 19.5 GeV (CMS). CMS also searched for the narrow resonances in the mass range 16.5 – 27 GeV. However, none of these studies revealed reliable signs of a resonance with properties expected for the exotic $bb\bar{b}\bar{b}$ state in the given process and at such energies.

The paper is organized as follows. In Sec. 2 we give a description and physical justification of the model for studying these tetraquark structures. In Sec. 3 we describe the relativistic quark model and its application to the calculation of the tetraquark mass spectra. In Sec. 4 we present the results of our calculations. In Sec. 5 we analyze our predictions comparing them with the thresholds for the strong fall-apart decays. In Sec. 6 we give a comparison of our results with the predictions of other scientific groups. Finally, in Sec. 7 the results and conclusions are summarized.

2. Model description of fully-heavy tetraquarks

Tetraquark is a bound state of two quarks and two antiquarks. There are 6 flavors of quarks, and according to their masses they can be divided into two groups: light (with the current masses less than the $\Lambda_{\text{QCD}} \approx 200$ MeV, quark confinement energy) and heavy (with masses larger than Λ_{QCD}) quarks. Light quarks are the u -quark with mass $2.16^{+0.49}_{-0.26}$ MeV, d -quark with mass $4.67^{+0.48}_{-0.17}$ MeV and s -quark with mass $93.4^{+8.6}_{-3.4}$ MeV. Heavy quarks are the c -quark with mass 1.27 ± 0.02 GeV, b -quark with mass $4.18^{+0.03}_{-0.02}$ GeV and t -quark with mass 172.69 ± 0.30 GeV [2]. We will focus on the fully-heavy tetraquarks. However, the t -quark is special. It is almost two orders of magnitude heavier than other heavy quarks, and thus it quickly decays via the weak interaction, not having enough time to form a bound state [13]. Therefore, we will not consider it.

From the two flavors of quarks and antiquarks, many combinations can be made. We have already done calculations for the ground states masses for all possible compositions [14,15]. However, given the large number of possible excited states, it is more rational to select and study those combinations that are easier to detect experimentally. The most convenient of these are the symmetric compositions: fully-charmed $cc\bar{c}\bar{c}$, doubly charmed-bottom $cb\bar{c}\bar{b}$, and fully-bottom $bb\bar{b}\bar{b}$ tetraquarks. The reason for the preference of such combinations is that the tetraquarks are formed from the closely produced quark and antiquark pairs. Thus the formation of these states requires the production of only

two pairs ($2 \times c\bar{c}$, $c\bar{c} + b\bar{b}$ and $2 \times b\bar{b}$) while the formation of other combinations requires the production of at least three pairs, which is a less probable event.

We consider the tetraquark as a bound state of a diquark QQ' and an antiquark $\bar{Q}\bar{Q}'$. This model is not new and is widely used in the hadron spectroscopy, giving good agreement between the calculations (for example, baryon masses) and experiments. Also theoretically predicted spectrum of possible baryon excitations in the genuine three body picture is much wider than the experimentally observed one. The quark-diquark model of baryons, on the other hand, freezes some degrees of freedom and imposes the necessary restrictions that bring the theory into better agreement with experiment [16,17].

Another widely used model for the tetraquarks description is a molecular picture. We consider such a picture of fully-heavy tetraquarks significantly less probable. Indeed, in this case the meson molecule model has the following main problems. The interaction between mesons in a molecule is either due to the Van der Waals forces, or through the exchange of another meson containing the same quarks as in the molecule. The Van der Waals forces are weak in general and cannot provide sufficient binding. In the fully-heavy tetraquarks only heavy mesons can be exchanged: $c\bar{c}$, $c\bar{b}$, $b\bar{c}$, $b\bar{b}$. Such interaction is described by the Yukawa potential and its strength decreases with the increasing mass of the exchanged meson. Therefore, such potential can provide a weak coupling in the case of the exchange of the light mesons, like pions ($M_{\pi^\pm} = 139.57$ MeV [2]), but in the considered case ($M_{min} = M_{\eta_c} = 2983.9 \pm 0.4$ MeV [2]) the coupling will be vanishingly small.

In the diquark consideration one must take into account that a (anti)diquark is a bound system of fermions, and therefore must obey the generalized Pauli principle: the complete wave function of a (anti)diquark must be antisymmetric. The diquark color representation can be either antitriplet (the antisymmetric color wave function) or sextet (the symmetric color wave function). But in the case of sextet the interaction potential between the quarks within the diquark is repulsive and thus corresponding diquark cannot be a bound state, which we consider inappropriate for our problem. The above argument applies to the antiquark. In the following we consider only color antitriplet diquarks. This means that if a (anti)diquark is composed of (anti)quarks of the same flavor (the symmetric flavor wave function), it can only have the symmetric spin wave function, thus being in the axialvector (A) state. If a diquark consists of quarks of different flavors, it can be either in the axialvector (A) or scalar (S) state.

3. Relativistic diquark-antidiquark model

For the calculation of the masses of tetraquarks, we use the relativistic quark model based on the quasipotential approach and the diquark-antidiquark picture of tetraquarks. In this approach the masses of tetraquarks are the solutions of the relativistic Schrödinger-type quasipotential equation [18–20]. This equation describes the bound state of two particles in a given quasipotential. We first apply it to the quark-quark system forming a diquark and then to the diquark-antidiquark system forming a tetraquark [21,22]:

$$\left(\frac{b^2(M)}{2\mu_R(M)} - \frac{\mathbf{p}^2}{2\mu_R(M)} \right) \Psi_{T,d}(\mathbf{p}) = \int \frac{d^3q}{(2\pi)^3} V(\mathbf{p}, \mathbf{q}; M) \Psi_{T,d}(\mathbf{q}). \quad (1)$$

Here \mathbf{p} is a vector of the relative momentum, M is the mass of the bound state, μ_R is the relativistic reduced mass of the constituents given by

$$\mu_R = \frac{E_1 E_2}{E_1 + E_2} = \frac{M^4 - (m_1^2 - m_2^2)^2}{4M^3}, \quad (2)$$

where $m_{1,2}$ are masses of the constituents and $E_{1,2}$ are the on-mass-shell energies of constituents:

$$E_{1,2} = \frac{M^2 - m_{2,1}^2 + m_{1,2}^2}{2M}. \quad (3)$$

$b^2(M)$ is the on-mass-shell relative momentum in the center-of-mass system squared:

$$b^2(M) = \frac{[M^2 - (m_1 + m_2)^2][M^2 - (m_1 - m_2)^2]}{4M^2}, \quad (4)$$

$\Psi_{T,d}(\mathbf{p})$ are the bound state wave functions, $V(\mathbf{p}, \mathbf{q}; M)$ is the quasipotential operator of the constituents.

The equation (1) is relativistic. On the left hand side it contains relativistic kinematics: the reduced mass of the bound state μ_R and the on-mass-shell relative momentum $b^2(M)$ are functions of the bound state mass M (Eq. (2)). The relativistic dynamics is contained on the right hand side of the Eq. (1), in the quasipotential $V(\mathbf{p}, \mathbf{q}; M)$. The quasipotential is constructed with the help of the off-mass-shell scattering amplitude, projected onto the positive-energy states and contains all relativistic spin-independent and spin-dependent contributions.

Constructing the quasipotential of the quark-quark interaction, we assume that the effective interaction is the sum of the usual one-gluon exchange term with the mixture of the long-range vector and scalar linear confining potentials, where the vector confining potential vertex contains the additional Pauli term. Due to the difference in the QQ' and $\bar{Q}\bar{Q}'$ color states the quark-quark interaction quasipotential is considered to be $V_{QQ'} = \frac{1}{2}V_{\bar{Q}\bar{Q}'}$ of the quark-antiquark interaction quasipotential [16] and is given by

$$V(\mathbf{p}, \mathbf{q}; M) = \bar{u}_1(p)\bar{u}_2(-p)\mathcal{V}(\mathbf{p}, \mathbf{q}; M)u_1(q)u_2(-q), \quad (5)$$

with

$$\begin{aligned} \mathcal{V}(\mathbf{p}, \mathbf{q}; M) &= \mathcal{V}_{\text{OGE}} + \mathcal{V}_{\text{conf.}}^V + \mathcal{V}_{\text{conf.}}^S \\ &= \frac{1}{2} \left[\underbrace{\frac{4}{3}\alpha_s D_{\mu\nu}(\mathbf{k})\gamma_1^\mu\gamma_2^\nu}_{\text{one-gluon-exchange}} + \underbrace{V_{\text{conf.}}^V(\mathbf{k})\Gamma_1^\mu(\mathbf{k})\Gamma_{2;\mu}(-\mathbf{k}) + V_{\text{conf.}}^S(\mathbf{k})}_{\text{confinement}} \right]. \end{aligned} \quad (6)$$

Here $\mathbf{k} = \mathbf{p} - \mathbf{q}$, $\gamma_l^{\mu,\nu}$ and $u_l^\lambda(p)$ are the Dirac matrices and spinors:

$$u_l^\lambda(p) = \sqrt{\frac{\varepsilon_l(p) + m_l}{2\varepsilon_l(p)}} \left(\frac{1}{\varepsilon_l(p) + m_l} \right) \chi^\lambda, \quad l = 1, 2, \quad (7)$$

where $\varepsilon_l(p)$ is the quark energy:

$$\varepsilon_l(p) = \sqrt{m_l^2 + \mathbf{p}^2}, \quad l = 1, 2, \quad (8)$$

σ and χ^λ are the Pauli matrices and spinors:

$$\chi^\lambda = \begin{pmatrix} 1 \\ 0 \end{pmatrix}, \begin{pmatrix} 0 \\ 1 \end{pmatrix}, \quad \lambda = 1, 2. \quad (9)$$

α_s is the running QCD coupling constant with freezing [23,24]:

$$\alpha_s(\mu^2) = \frac{4\pi}{(11 - \frac{2}{3}\eta_f) \ln[\frac{\mu^2 + M_{BG}^2}{\Lambda^2}]}, \quad (10)$$

$$\begin{cases} \mu = \frac{2m_1m_2}{(m_1+m_2)}, \\ M_{BG} = 2.24\sqrt{A} = 0.95 \text{ GeV}, \\ \Lambda = 414 \text{ MeV}, \\ \eta_f = \begin{cases} 4, & Q = Q' = c, \\ 5, & Q, Q' = c, b, \end{cases} \end{cases} \quad (11)$$

where the scale μ is chosen to be equal to the reduced constituents mass, M_{BG} is the background mass, Λ is the parameter of the running coupling constant obtained from the analysis of meson mass spectra and η_f is the number of open flavors. $D_{\mu\nu}(\mathbf{k})$ is the gluon propagator in the Coulomb gauge:

$$\begin{cases} D^{00}(\mathbf{k}) = -\frac{4\pi}{\mathbf{k}^2}, \\ D^{ij}(\mathbf{k}) = -\frac{4\pi}{\mathbf{k}^2} \left(\delta^{ij} - \frac{k^i k^j}{\mathbf{k}^2} \right), & i, j = \overline{1,3}. \\ D^{0i} = D^{i0} = 0, \end{cases} \quad (12)$$

Γ_l^μ is the effective long-range vector interaction vertex [25], it contains both Dirac and Pauli terms:

$$\Gamma_{l;\mu}(\mathbf{k}) = \gamma_\mu + \frac{i\kappa}{2m_l} \sigma_{\mu\nu} \tilde{k}^\nu, \quad \tilde{k} = (0, \mathbf{k}), \quad l = 1, 2, \quad (13)$$

where $\sigma_{\mu\nu}$ is the commutator of the Dirac matrices, κ is the long-range anomalous chromomagnetic moment of quarks and $\frac{i\kappa}{2m_l} \sigma_{\mu\nu} \tilde{k}^\nu$ is the anomalous chromomagnetic interaction. $V_{\text{conf.}}^{v,s}$ are the vector and scalar confining potentials which in the nonrelativistic limit in configuration space (consistent with the lattice calculations) have the form

$$\begin{aligned} V_{\text{conf.}}^V(r) &= (1 - \varepsilon) V_{\text{conf.}}(r), \\ V_{\text{conf.}}^S(r) &= \varepsilon V_{\text{conf.}}(r), \\ V_{\text{conf.}}^V(r) + V_{\text{conf.}}^S(r) &= V_{\text{conf.}}(r) = Ar + B, \end{aligned} \quad (14)$$

where ε is the mixing coefficient. Therefore in the nonrelativistic limit the QQ' quasipotential reduces to:

$$V_{QQ'}^{\text{NR}}(r) = \frac{1}{2} V_{QQ'}^{\text{NR}}(r) = \frac{1}{2} \left(-\frac{4}{3} \frac{\alpha_s}{r} + Ar + B \right), \quad (15)$$

reproducing the usual Cornell potential. Thus, our quasipotential can be viewed as its relativistic generalization. It contains both spin-independent and spin-dependent relativistic contributions.

Constructing the diquark-antidiquark quasipotential, we use the same assumptions about the structure of the short- and long-range interactions. We also take into account the finite size of the diquarks and their integer spin. The quasipotential then is given by [22,26]:

$$\begin{aligned} V(\mathbf{p}, \mathbf{q}; M) &= \underbrace{\frac{\langle d(\mathcal{P}) | J_\mu | d(\mathcal{Q}) \rangle}{2\sqrt{E_d} \sqrt{E_d}} \frac{4}{3} \alpha_s D^{\mu\nu}(\mathbf{k}) \frac{\langle d'(\mathcal{P}') | J_\nu | d'(\mathcal{Q}') \rangle}{2\sqrt{E_{d'}} \sqrt{E_{d'}}}}_{\text{diquark-gluon interaction}} \\ &+ \underbrace{\Psi_d^*(\mathcal{P}) \Psi_{d'}^*(\mathcal{P}') [J_{d;\mu} J_{d'}^\mu V_{\text{conf.}}^V(\mathbf{k}) + V_{\text{conf.}}^S(\mathbf{k})] \Psi_d(\mathcal{Q}) \Psi_{d'}(\mathcal{Q}')}_{\text{confinement}}. \end{aligned} \quad (16)$$

Here d and d' denote the diquark and antidiquark, $\mathcal{Q}^{(\prime)} = (E_{d^{(\prime)}} \pm \mathbf{q})$ and $\mathcal{P}^{(\prime)} = (E_{d^{(\prime)}} \pm \mathbf{p})$ are the initial and final diquark momenta respectively, $k = \mathcal{P} - \mathcal{Q}$, $E_{d,d'}$ are the on-shell diquark energies (similar to Eq. (3)):

$$\begin{cases} E_d = \frac{M^2 - M_{d'}^2 + M_d^2}{2M}, \\ E_{d'} = \frac{M^2 - M_d^2 + M_{d'}^2}{2M}, \end{cases} \quad (17)$$

where $M_{d,d'}$ are the diquark and antidiquark masses. $\Psi_d(p)$ is the diquark wave function:

$$\Psi_d(p) = \begin{cases} 1, & \text{scalar} \\ \varepsilon_d(p), & \text{axialvector} \end{cases} \quad \text{diquarks}, \quad (18)$$

where $\epsilon_d(p)$ is the polarization vector of an axialvector diquark with momentum \mathbf{p} :

$$\epsilon_d(p) = \left(\frac{(\epsilon_d \mathbf{P})}{M_d}, \epsilon_d + \frac{(\epsilon_d \mathbf{P}) \mathbf{P}}{M_d(M_d + E_d(p))} \right), \quad (19)$$

$$\epsilon_d^\mu(p) p_\mu = 0,$$

where $E_d(p)$ is the diquark energy (similar to Eq. (8)):

$$E_d(p) = \sqrt{M_d^2 + \mathbf{p}^2}. \quad (20)$$

$J_{d;\mu}$ is the effective long-range vector interaction vertex of the diquark:

$$J_{d;\mu} = \begin{cases} \frac{(\mathcal{P}+\mathcal{Q})_\mu}{2\sqrt{E_d}\sqrt{E_d}}, & \text{scalar} \\ -\frac{(\mathcal{P}+\mathcal{Q})_\mu}{2\sqrt{E_d}\sqrt{E_d}} + \frac{i\mu_d}{2M_d} \sum_\nu \tilde{k}_\nu, & \text{axialvector} \end{cases} \quad \text{diquarks,} \quad (21)$$

$$\mu_d = 0, \quad (22)$$

where μ_d is the total chromomagnetic moment of the diquark, which we choose equal to zero to vanish the long-range chromomagnetic interaction. $(\sum_{\rho\sigma})_\mu^\nu$ is a fully antisymmetric tensor:

$$(\sum_{\rho\sigma})_\mu^\nu = -i(g_{\mu\rho}\delta_\sigma^\nu - g_{\mu\sigma}\delta_\rho^\nu). \quad (23)$$

$\langle d(\mathcal{P}) | J_\mu | d(\mathcal{Q}) \rangle$ is the diquark-gluon interaction vertex (Fig. 1), which accounts for the internal structure of the diquark and leads to the emergence of the form factor $F(r)$ smearing the one-gluon exchange potential [21]:

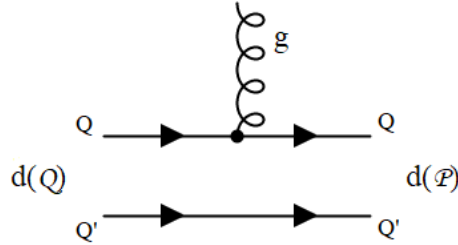


Figure 1. Feynman diagram of the gluon emission by a quark in a diquark.

$$\langle d(\mathcal{P}) | J_\mu | d(\mathcal{Q}) \rangle = \int \frac{d^3 p d^3 q}{(2\pi)^6} \bar{\Psi}_d^\mathcal{P}(\mathbf{p}) \Gamma_\mu(\mathbf{p}, \mathbf{q}) \Psi_d^\mathcal{Q}(\mathbf{q}). \quad (24)$$

Here J_μ is the quark current:

$$J_\mu = \bar{Q} \gamma_\mu Q, \quad (25)$$

where Q, \bar{Q} denotes the initial and final states of the quark, respectively. $\Gamma_\mu(\mathbf{p}, \mathbf{q})$ is the vertex function of the diquark interaction with the gluon field [27,28]:

$$\Gamma^\mu(\mathbf{p}, \mathbf{q}) = \bar{u}_{Q_1}(p_1) \gamma^\mu u_{Q_1}(q_1) (2\pi)^3 \delta(\mathbf{p}_2 - \mathbf{q}_2) + \bar{u}_{Q_2}(p_2) \gamma^\mu u_{Q_2}(q_2) (2\pi)^3 \delta(\mathbf{p}_1 - \mathbf{q}_1), \quad (26)$$

$$\left\{ \begin{array}{l} q_l = \varepsilon_l(q) \frac{Q}{M_d(q)} \pm \sum_{i=1}^3 n^{(i)}(\mathcal{Q}) q^i, \\ p_l = \varepsilon_l(p) \frac{P}{M_d(p)} \pm \sum_{i=1}^3 n^{(i)}(\mathcal{P}) p^i, \\ n^{(i)\mu}(\mathcal{Q}) = \left\{ \frac{Q^i}{M_d}, \delta_{ij} + \frac{Q^i Q^j}{M_d(q)(E_d(\mathcal{Q}) + M_d(q))} \right\}, \\ M_d(q) = \varepsilon_1(q) + \varepsilon_2(q), \end{array} \right. \quad l = 1, 2 \equiv Q, Q'. \quad (27)$$

To take into account the finite size of the diquark, it is necessary to calculate the matrix elements of quark currents between diquarks $\langle d(\mathcal{P})|J_\mu|d(\mathcal{Q}) \rangle$. These matrix elements are elastic (diagonal) and can be parametrized by the set of form factors $h_{+,1,2,3}(k^2)$ [21]. For a scalar diquark:

$$\langle S(\mathcal{P})|J_\mu|S(\mathcal{Q}) \rangle = h_+(k^2)(\mathcal{P} + \mathcal{Q})_\mu, \quad (28)$$

For an axialvector diquark:

$$\begin{aligned} \langle A(\mathcal{P})|J_\mu|A(\mathcal{Q}) \rangle = & -h_1(k^2) \left[\epsilon_d^*(\mathcal{P}) \cdot \epsilon_d(\mathcal{Q}) \right] (\mathcal{P} + \mathcal{Q})_\mu \\ & + h_2(k^2) \left\{ \left[\epsilon_d^*(\mathcal{P}) \cdot \mathcal{Q} \right] \epsilon_{d;\mu}(\mathcal{Q}) + \left[\epsilon_d(\mathcal{Q}) \cdot \mathcal{P} \right] \epsilon_{d;\mu}^*(\mathcal{P}) \right\} \\ & + h_3(k^2) \frac{1}{M_A^2} \left[\epsilon_d^*(\mathcal{P}) \cdot \mathcal{Q} \right] \left[\epsilon_d(\mathcal{Q}) \cdot \mathcal{P} \right] (\mathcal{P} + \mathcal{Q})_\mu, \end{aligned} \quad (29)$$

where M_A is the mass of the axialvector diquark.

The calculation shows that [16]:

$$\begin{cases} h_+(k^2) = h_1(k^2) = h_2(k^2) = F(\mathbf{k}^2), \\ h_3(k^2) = 0, \end{cases} \quad (30)$$

where $F(\mathbf{k}^2)$ is the form factor in the momentum space:

$$\begin{aligned} F(\mathbf{k}^2) = & \frac{\sqrt{M_d E_d}}{M_d + E_d} \int \frac{d^3 p}{(2\pi)^3} \left\{ \left[\bar{\Psi}_d \left(\mathbf{p} + \frac{2\varepsilon_{Q_2}(p)}{M_d + E_d} \mathbf{k} \right) \sqrt{\frac{\varepsilon_{Q_1}(p) + m_{Q_1}}{\varepsilon_{Q_1}(p+k) + m_{Q_1}}} \right. \right. \\ & \times \left. \left(\frac{\varepsilon_{Q_1}(p+k) + \varepsilon_{Q_1}(p)}{2\sqrt{\varepsilon_{Q_1}(p+k)\varepsilon_{Q_1}(p)}} + \frac{\mathbf{p}\mathbf{k}}{2(\varepsilon_{Q_1}(p) + m_{Q_1})\sqrt{\varepsilon_{Q_1}(p+k)\varepsilon_{Q_1}(p)}} \right) \Psi_d(\mathbf{p}) \right] \\ & + \left[\bar{\Psi}_d \left(\mathbf{p} + \frac{2\varepsilon_{Q_1}(p)}{M_d + E_d} \mathbf{k} \right) \sqrt{\frac{\varepsilon_{Q_2}(p) + m_{Q_2}}{\varepsilon_{Q_2}(p+k) + m_{Q_2}}} \right. \\ & \left. \left. \times \left(\frac{\varepsilon_{Q_2}(p+k) + \varepsilon_{Q_2}(p)}{2\sqrt{\varepsilon_{Q_2}(p+k)\varepsilon_{Q_2}(p)}} + \frac{\mathbf{p}\mathbf{k}}{2(\varepsilon_{Q_2}(p) + m_{Q_2})\sqrt{\varepsilon_{Q_2}(p+k)\varepsilon_{Q_2}(p)}} \right) \Psi_d(\mathbf{p}) \right] \right\}. \end{aligned} \quad (31)$$

The form factor $F(r)$ is determined by the Fourier transform of the $\frac{F(\mathbf{k}^2)}{\mathbf{k}^2}$ which is then multiplied by r . Numerical calculations show that it can be parameterized with high accuracy as [21]:

$$F(r) = 1 - e^{-\xi r - \zeta r^2}, \quad (32)$$

the accuracy of this approximation is shown in Fig. 2.

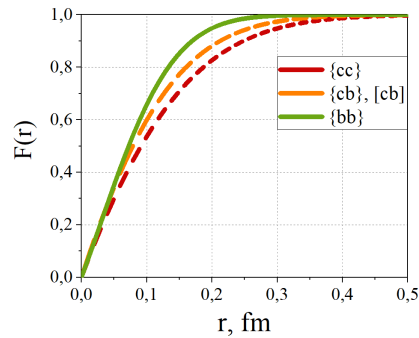


Figure 2. Form factors $F(r)$ for the various doubly heavy diquarks. $\{Q, Q'\}$ denotes axialvector and $[Q, Q']$ denotes scalar diquarks, respectively.

Finally, we obtain the diquark-antidiquark interaction potential [15,26]:

$$\begin{aligned}
V(r) = & \left[V_{\text{Coul.}}(r) + V_{\text{conf.}}(r) + \frac{1}{E_1 E_2} \left\{ \mathbf{p} \left[V_{\text{Coul.}}(r) + V_{\text{conf.}}^V(r) \right] \mathbf{p} \right. \right. \\
& \left. \left. - \frac{1}{4} \Delta V_{\text{conf.}}^V(r) + V'_{\text{Coul.}}(r) \frac{\mathbf{L}^2}{2r} \right\} \right]_a \quad (a) \\
& + \left[\left\{ \frac{1}{2} \left[\frac{1}{E_1(E_1 + M_1)} + \frac{1}{E_2(E_2 + M_2)} \right] \frac{V'_{\text{Coul.}}(r)}{r} \right. \right. \\
& - \frac{1}{2} \left[\frac{1}{M_1(E_1 + M_1)} + \frac{1}{M_2(E_2 + M_2)} \right] \frac{V'_{\text{conf.}}(r)}{r} + \frac{\mu_d}{4} \left[\frac{1}{M_1^2} + \frac{1}{M_2^2} \right] \frac{V'^V_{\text{conf.}}(r)}{r} \\
& + \frac{1}{E_1 E_2} \left[V'_{\text{Coul.}}(r) + \frac{\mu_d}{4} \left(\frac{E_1}{M_1} + \frac{E_2}{M_2} \right) V'^V_{\text{conf.}}(r) \right] \frac{1}{r} \left. \right\} \mathbf{L}(\mathbf{S}_1 + \mathbf{S}_2) \\
& + \left\{ \frac{1}{2} \left[\frac{1}{E_1(E_1 + M_1)} - \frac{1}{E_2(E_2 + M_2)} \right] \frac{V'_{\text{Coul.}}(r)}{r} \right. \\
& - \frac{1}{2} \left[\frac{1}{M_1(E_1 + M_1)} - \frac{1}{M_2(E_2 + M_2)} \right] \frac{V'_{\text{conf.}}(r)}{r} + \frac{\mu_d}{4} \left[\frac{1}{M_1^2} - \frac{1}{M_2^2} \right] \frac{V'^V_{\text{conf.}}(r)}{r} \\
& + \frac{1}{E_1 E_2} \frac{\mu_d}{4} \left(\frac{E_1}{M_1} - \frac{E_2}{M_2} \right) \frac{V'^V_{\text{conf.}}(r)}{r} \left. \right\} \mathbf{L}(\mathbf{S}_1 - \mathbf{S}_2) \right]_b \quad (b) \\
& + \left[\frac{1}{3E_1 E_2} \left\{ \frac{1}{r} V'_{\text{Coul.}}(r) - V''_{\text{Coul.}}(r) + \frac{\mu_d^2}{4} \frac{E_1 E_2}{M_1 M_2} \left(\frac{1}{r} V'^V_{\text{conf.}}(r) - V''^V_{\text{conf.}}(r) \right) \right\} \right. \\
& \left. \times \left[\frac{3}{r^2} (\mathbf{S}_1 \mathbf{r}) (\mathbf{S}_2 \mathbf{r}) - \mathbf{S}_1 \mathbf{S}_2 \right] \right]_c \quad (c) \\
& + \left[\frac{2}{3E_1 E_2} \left\{ \Delta V_{\text{Coul.}}(r) + \frac{\mu_d^2}{4} \frac{E_1 E_2}{M_1 M_2} \Delta V_{\text{conf.}}^V(r) \right\} \mathbf{S}_1 \mathbf{S}_2 \right]_{d'} \quad (d) \\
& \quad (33)
\end{aligned}$$

where \mathbf{p} is the relative momentum, $M_{1,2}$ and $E_{1,2}$ are the masses and energies of the diquark and antidiquark, μ_d is the total chromomagnetic moment of the diquark (we chose it to be zero), \mathbf{S}_d is the axialvector diquark spin, \mathbf{L} is the relative orbital momentum of the system, $V_{\text{conf.}}$ is the confining potential in the nonrelativistic limit:

$$V_{\text{conf.}} = V_{\text{conf.}}^V + V_{\text{conf.}}^S = (1 - \varepsilon)(Ar + B) + \varepsilon(Ar + B) = Ar + B, \quad (34)$$

where ε are the scalar and vector confinement mixing coefficient, and the Coulomb potential $V_{\text{Coul.}}(r)$ is taken to be

$$V_{\text{Coul.}}(r) \equiv -\frac{4}{3} \alpha_s \frac{F_1(r) F_2(r)}{r}. \quad (35)$$

$F_{1,2}(r)$ are the form factors that take into account diquark sizes (Eq. (32)).

In Eq. (33) we explicitly separated the spin-independent (a) and spin-dependent terms: (b) for the spin-orbit, (c) for the tensor and (d) for the spin-spin interactions.

First, we calculate the masses and wave functions of the doubly-heavy (anti)diquarks as the bound (anti)quark-(anti)quark states. It is done by solving Eq. (1) with the quasipotential (5), (6)-(14) numerically. Then the masses of the tetraquarks and their wave functions are obtained for the bound diquark-antidiquark states with the same method.

Parameters such as the confinement potential mixing coefficient ε , anomalous chromomagnetic moment κ , parameter of the running coupling constant Λ , confining potential parameters A, B and quark masses $m_{c,b}$ are taken from our previous works on the study of the properties of mesons and baryons [25,29–31] and are given in the Table 1. The diquark masses $M_{cc,cb,bb}$ and the parameters of their form factors ξ and ζ have already been calculated earlier [21,26] and are given in the Table 2.

Table 1. Parameters of the model [25,29–31].

m_c, GeV	m_b, GeV	A, GeV^2	B, GeV	Λ, MeV	ε	κ
1.55	4.88	0.18	-0.3	414	-1	-1

Table 2. Masses $M_{QQ'}$ and form factor parameters ξ, ζ of diquarks. d is the axialvector (A) or scalar (S) diquark. $[Q, Q']$ and $\{Q, Q'\}$ denote combinations of quarks antisymmetric and symmetric in flavor, respectively [21,26].

QQ'	d	$Q = c$			$Q = b$		
		M_{cQ}, MeV	ξ, GeV	ζ, GeV^2	M_{bQ}, MeV	ξ, GeV	ζ, GeV^2
$[Q, c]$	S				6519	1.50	0.59
$\{Q, c\}$	A	3226	1.30	0.42	6526	1.50	0.59
$\{Q, b\}$	A	6526	1.50	0.59	9778	1.30	1.60

4. Masses of fully-heavy tetraquarks

The calculated mass spectra of fully-heavy tetraquarks are given in Table 3. Masses of the ground states (1S) of all possible nine compositions of fully-heavy tetraquarks (including symmetrical: $cc\bar{c}\bar{c}, cb\bar{c}\bar{b}, bb\bar{b}\bar{b}$, “mirrored”: $cb\bar{b}\bar{b}, bb\bar{c}\bar{c}$ and nonsymmetrical: $cc\bar{c}\bar{b}, cb\bar{c}\bar{c}, cb\bar{b}\bar{b}, bb\bar{c}\bar{b}$) have already been calculated in our previous work [14].

As it already have been discussed in Sec. 2, a scalar (anti)diquark can be a part of a tetraquark only if the (anti)quarks that form it have different flavors. This means that the $cc\bar{c}\bar{c}$ and $bb\bar{b}\bar{b}$ tetraquarks can consist only of an axialvector diquarks and antidiquarks, while $cb\bar{c}\bar{b}$ can also consist of a scalar and a mixture of axialvector and scalar diquarks and antidiquarks. As the result, we get more possible states for $cb\bar{c}\bar{b}$: additional 12 mixed and 6 scalar states are added to 32 axialvector states.

Table 3. Masses $M_{QQ'Q\bar{Q}'}$ of the ground (1S) and excited (1P, 2S, 1D, 2P, 3S) $cc\bar{c}\bar{c}$, $cb\bar{c}\bar{b}$, $bb\bar{b}\bar{b}$ states. d and \bar{d}' are the axialvector (A) or scalar (S) diquark and antidiquark, respectively. S is the total spin of the diquark-antidiquark system. All masses are given in MeV.

$d\bar{d}'$	State	S	J^{PC}	$M_{cc\bar{c}\bar{c}}$	$M_{cb\bar{c}\bar{b}}$	$M_{bb\bar{b}\bar{b}}$	
$A\bar{A}$	1S	0	0^{++}	6190	12838	19315	
		1	1^{+-}	6271	12855	19320	
		2	2^{++}	6367	12883	19331	
	1P	0	1^{--}	6631	13103	19536	
			0^{-+}	6628	13100	19533	
			1^{-+}	6634	13103	19535	
		1	2^{-+}	6644	13108	19539	
			1^{--}	6635	13103	19534	
			2^{--}	6648	13109	19538	
	2S	0	0^{++}	6782	13247	19680	
		1	1^{+-}	6816	13256	19682	
		2	2^{++}	6868	13272	19687	
	1D	0	2^{++}	6921	13306	19715	
			1^{+-}	6909	13299	19710	
			2^{+-}	6920	13304	19714	
		1	3^{+-}	6932	13311	19720	
			0^{++}	6899	13293	19705	
			1^{++}	6904	13296	19707	
			2	2^{++}	6915	13301	19711
				3^{++}	6929	13308	19717
				4^{++}	6945	13317	19724
		2P	0	1^{--}	7091	13428	19820
				0^{-+}	7100	13431	19821
				1^{-+}	7099	13431	19821
	1		2^{-+}	7098	13431	19822	
			1^{--}	7113	13434	19823	
			2^{--}	7113	13435	19823	
2	3^{--}	7112	13436	19824			
	0	0^{++}	7259	13558	19941		
		1	1^{+-}	7287	13566	19943	
2		2^{++}	7333	13580	19947		
$\frac{1}{\sqrt{2}}(A\bar{S} \pm S\bar{A})$	1S		$1^{+\pm}$		12863		
			$0^{-\pm}$		13096		
	1P		$1^{-\pm}$		13099		
			$2^{-\pm}$		13104		
	2S		$1^{+\pm}$		13257		
	1D	1	$1^{+\pm}$		13293		
			$2^{+\pm}$		13298		
			$3^{+\pm}$		13305		
	2P	1	$0^{-\pm}$		13426		
			$1^{-\pm}$		13426		
			$2^{-\pm}$		13427		
	3S		$1^{+\pm}$		13566		
$S\bar{S}$	1S		0^{++}		12856		
	1P		1^{--}		13095		
	2S		0^{++}		13250		
	1D	0	2^{++}		13293		
	2P		1^{--}		13420		
	3S		0^{++}		13559		

5. Threshold analysis

If a mass of the tetraquark exceeds the sum of the masses of a meson pair composed of the same flavor quarks and antiquarks, and its decay is not forbidden by quantum

numbers (spin-parity J^{PC}), then the tetraquark will decay into this meson pair through the quark rearrangement via the strong interaction. This is the so-called fall-apart process, which rate is governed by the difference of the tetraquark and threshold masses. If a mass of the tetraquark lies below the corresponding threshold, the decay is possible due to the heavy quark-antiquark annihilation into gluons or a radiative decay, but such processes are suppressed, making these tetraquarks narrow states.

In Tables 4-8 comparisons of mass spectra of fully heavy tetraquarks, calculated by us (Table 3), with the meson pair decay thresholds are given. The values of the phase volume Δ are of special interest:

$$\Delta = M_{QQ'\bar{Q}\bar{Q}'} - M_{thr}, \quad (36)$$

where $M_{QQ'\bar{Q}\bar{Q}'}$ is the tetraquark mass and M_{thr} is the meson pair decay threshold. We are interested in the most probable decay modes for each tetraquark. They, in turn, correspond to the largest of possible values of Δ : Δ_{max} . Therefore, in Tables 4-8 we compare tetraquark masses not with all possible thresholds, but only with the lowest ones ($[M_{thr}]_{min} \rightarrow \Delta_{max} \rightarrow$ more probable decay mode).

Table 4. Masses M of the ground (1S) and excited (1P, 2S, 1D, 2P, 3S) $cc\bar{c}\bar{c}$ states composed from the axialvector diquarks (Table 3) and the corresponding meson-meson thresholds. d and \bar{d}' are the axialvector (A) or scalar (S) diquark and antidiquark, respectively. S is the total spin of the diquark-antidiquark system. M_{thr} is the corresponding meson-meson threshold [2]. Δ is the difference between the tetraquark mass and threshold: $\Delta = M - M_{thr}$. All masses are given in MeV. For the states with the maximum Δ (corresponding to lightest threshold, main decay channel) less than 300 MeV, all possible thresholds and their Δ are given. For the states with maximum Δ above 300 MeV, only the lightest thresholds are shown. The states with maximum Δ less than 100 MeV are additionally highlighted in violet as most promising to be stable. The states with negative maximum Δ are highlighted in red for the same reason. We also give thresholds with a small negative Δ , since we do not take into account the errors of theoretical calculations. The candidates for the states recently observed by LHCb [5], CMS [6] and ATLAS [7] are highlighted in color: turquoise for X(6200) (ATLAS), emerald for X(6400) (LHCb) and X(6600) (CMS, ATLAS), green for X(6900) (LHCb, CMS, ATLAS), blue for X(7200) (LHCb, ATLAS) and X(7300) (CMS). Additionally all di- J/ψ and di- $Y(1S)$ (in similar table for $bb\bar{b}\bar{b}$ states) thresholds are shown in bold since this meson pairs are easiest to study in experiments.

$QQ\bar{Q}\bar{Q}$	$d\bar{d}'$	State	S	J^{PC}	M	M_{thr}	Δ	Meson pair
$cc\bar{c}\bar{c}$	$A\bar{A}$	1S	0	0⁺⁺	6190	5968	222	$\eta_c(1S)\eta_c(1S)$
						6194	-4	$J/\psi(1S)J/\psi(1S)$
			1	1 ^{+−}	6271	6081	190	$\eta_c(1S)J/\psi(1S)$
			2	2⁺⁺	6367	6194	173	$J/\psi(1S)J/\psi(1S)$
		1P	0	1 ^{−−}	6631	6509	122	$\eta_c(1S)h_c(1P)$
						6512	119	$J/\psi(1S)\chi_{c0}(1P)$
						6608	23	$J/\psi(1S)\chi_{c1}(1P)$
				0 ^{−+}	6628	6399	229	$\eta_c(1S)\chi_{c0}(1P)$
						6622	6	$J/\psi(1S)h_c(1P)$
			1	1 ^{−+}	6634	6495	139	$\eta_c(1S)\chi_{c1}(1P)$
					6622	12	$J/\psi(1S)h_c(1P)$	
			2 ^{−+}	6644	6540	104	$\eta_c(1S)\chi_{c2}(1P)$	
					6622	22	$J/\psi(1S)h_c(1P)$	
					6509	126	$\eta_c(1S)h_c(1P)$	
	2	1 ^{−−}		6635	6512	123	$J/\psi(1S)\chi_{c0}(1P)$	
					6608	27	$J/\psi(1S)\chi_{c1}(1P)$	
					6653	-18	$J/\psi(1S)\chi_{c2}(1P)$	
		2			6608	6608	40	$J/\psi(1S)\chi_{c1}(1P)$
					6653	6653	-5	$J/\psi(1S)\chi_{c2}(1P)$
				2^{−−}	6648			
				6653	6653	-5	$J/\psi(1S)\chi_{c2}(1P)$	
			3^{−−}	6664	6653	11	$J/\psi(1S)\chi_{c2}(1P)$	

Table 4. Table continued.

QQ $\bar{Q}\bar{Q}$	d \bar{d}'	State	S	J ^{PC}	M	M _{thr}	Δ	Meson pair	
<i>cc$\bar{c}\bar{c}$</i>	<i>A\bar{A}</i>	2S	0	0 ⁺⁺	6782 ¹	5968	814	$\eta_c(1S)\eta_c(1S)$	
			1	1 ⁺⁻	6816	6081	735	$J/\psi(1S)J/\psi(1S)$	
			2	2 ⁺⁺	6868	6194	674	$J/\psi(1S)J/\psi(1S)$	
		1D	0	2 ⁺⁺	6921	6194	727	$J/\psi(1S)J/\psi(1S)$	
			1	1 ⁺⁻	6909	6081	828	$\eta_c(1S)J/\psi(1S)$	
				2 ⁺⁻	6920	6808	112	$\eta_c(1S)\psi_2(3823)$	
				3 ⁺⁻	6932	6827	105	$\eta_c(1S)\psi_3(3842)$	
			2	0 ⁺⁺	6899	6194	705	$J/\psi(1S)J/\psi(1S)$	
				1 ⁺⁺	6904	6194	710	$J/\psi(1S)J/\psi(1S)$	
				2 ⁺⁺	6915	6194	721	$J/\psi(1S)J/\psi(1S)$	
				3 ⁺⁺	6929	6921	8	$J/\psi(1S)\psi_2(3823)$	
				4 ⁺⁺	6945	6940	19	$J/\psi(1S)\psi_3(3842)$	
				4 ⁺⁺	6945	6940	5	$J/\psi(1S)\psi_3(3842)$	
			2P	0	1 ⁻⁻	7091	6509	582	$\eta_c(1S)h_c(1P)$
				1	0 ⁻⁺	7100	6399	701	$\eta_c(1S)\chi_{c0}(1P)$
		1 ⁻⁺			7099	6495	604	$\eta_c(1S)\chi_{c1}(1P)$	
		2 ⁻⁺			7098	6540	558	$\eta_c(1S)\chi_{c2}(1P)$	
		2		1 ⁻⁻	7113	6509	604	$\eta_c(1S)h_c(1P)$	
				2 ⁻⁻	7113	6608	505	$J/\psi(1S)\chi_{c1}(1P)$	
			3 ⁻⁻	7112	6653	459	$J/\psi(1S)\chi_{c2}(1P)$		
		3S	0	0 ⁺⁺	7259	5968	1291	$\eta_c(1S)\eta_c(1S)$	
			1	1 ⁺⁻	7287	6081	1206	$J/\psi(1S)J/\psi(1S)$	
			2	2 ⁺⁺	7333 ²	6194	1139	$J/\psi(1S)J/\psi(1S)$	

¹ Candidate only for the X(6600) state.² Candidate only for the X(7300) state.Table 5. Same as in Table 4 but for *cb $\bar{c}\bar{b}$* states composed from the axialvector (A) diquarks.

QQ $\bar{Q}\bar{Q}$	d \bar{d}'	State	S	J ^{PC}	M	M _{thr}	Δ	Meson pair	
<i>cb$\bar{c}\bar{b}$</i>	<i>A\bar{A}</i>	1S	0	0 ⁺⁺	12838	12383	455	$\eta_c(1S)\eta_b(1S)$	
			1	1 ⁺⁻	12855	12444	411	$\eta_c(1S)Y(1S)$	
			2	2 ⁺⁺	12883	12557	326	$J/\psi(1S)Y(1S)$	
		1P	0	1 ⁻⁻	13103	12875	12875	228	$\chi_{c0}(1P)Y(1S)$
						12883	12883	220	$\eta_c(1S)h_b(1P)$
						12924	12924	179	$h_c(1P)\eta_b(1S)$
						12956	12956	147	$J/\psi(1S)\chi_{b0}(1P)$
						12971	12971	132	$\chi_{c1}(1P)Y(1S)$
						12990	12990	113	$J/\psi(1S)\chi_{b1}(1P)$
			1	1 ⁻⁺	13103	13009	13009	94	$J/\psi(1S)\chi_{b2}(1P)$
						13016	13016	87	$\chi_{c2}(1P)Y(1S)$
						12813	12813	287	$\chi_{c0}(1P)\eta_b(1S)$
						12843	12843	257	$\eta_c(1S)\chi_{b0}(1P)$
						12986	12986	114	$h_c(1P)Y(1S)$
						12996	12996	104	$J/\psi(1S)h_b(1P)$
			2	2 ⁻⁺	13108	12877	12877	226	$\eta_c(1S)\chi_{b1}(1P)$
						12909	12909	194	$\chi_{c1}(1P)\eta_b(1S)$
						12986	12986	117	$h_c(1P)Y(1S)$
						12996	12996	107	$J/\psi(1S)h_b(1P)$
						12896	12896	212	$\eta_c(1S)\chi_{b2}(1P)$
						12955	12955	153	$\chi_{c2}(1P)\eta_b(1S)$
		12986	12986	122	12986	12986	122	12986	$h_c(1P)Y(1S)$

Table 5. Table continued.

QQQ \bar{Q}	d \bar{d}'	State	S	J ^{PC}	M	M _{thr}	Δ	Meson pair	
$cb\bar{c}\bar{b}$	$A\bar{A}$	1P	2	1^{--}	13103	12875	228	$\chi_{c0}(1P)Y(1S)$	
						12883	220	$\eta_c(1S)h_b(1P)$	
						12924	179	$h_c(1P)\eta_b(1S)$	
						12956	147	$J/\psi(1S)\chi_{b0}(1P)$	
						12971	132	$\chi_{c1}(1P)Y(1S)$	
						12990	113	$J/\psi(1S)\chi_{b1}(1P)$	
				13009	94	$J/\psi(1S)\chi_{b2}(1P)$			
				13016	87	$\chi_{c2}(1P)Y(1S)$			
				12971	138	$\chi_{c1}(1P)Y(1S)$			
				12990	119	$J/\psi(1S)\chi_{b1}(1P)$			
				13009	100	$J/\psi(1S)\chi_{b2}(1P)$			
				13016	93	$\chi_{c2}(1P)Y(1S)$			
		13009	107	$J/\psi(1S)\chi_{b2}(1P)$					
		13016	100	$\chi_{c2}(1P)Y(1S)$					
		2S	0	0^{++}	13247	12383	864	$\eta_c(1S)\eta_b(1S)$	
			1	1^{+-}	13256	12444	812	$\eta_c(1S)Y(1S)$	
			2	2^{++}	13272	12557	715	$J/\psi(1S)Y(1S)$	
			1D	0	2^{++}	13306	12557	749	$J/\psi(1S)Y(1S)$
				1	1^{+-}	13299	12444	855	$\eta_c(1S)Y(1S)$
					2^{+-}	13304	13148	156	$\eta_c(1S)Y_2(1D)$
		2	3^{+-}	13311	13222	82	$\psi_2(3823)\eta_b(1S)$		
			0^{++}	13293	13241	70	$\psi_3(3842)\eta_b(1S)$		
			1^{++}	13296	13283	910	$\eta_c(1S)\eta_b(1S)$		
			2^{++}	13301	12557	739	$J/\psi(1S)Y(1S)$		
			3	13261	3^{++}	13308	13261	47	$J/\psi(1S)Y_2(1D)$
						13284	13284	24	$\psi_2(3823)Y(1S)$
				13303	13303	5	$\psi_3(3842)Y(1S)$		
				13303	13303	14	$\psi_3(3842)Y(1S)$		
			2P	0	1^{--}	13428	12875	553	$\chi_{c0}(1P)Y(1S)$
				1	0^{-+}	13431	12813	618	$\chi_{c0}(1P)\eta_b(1S)$
		1^{-+}			13431	12877	554	$\eta_c(1S)\chi_{b1}(1P)$	
		2		2^{-+}	13431	12896	535	$\eta_c(1S)\chi_{b2}(1P)$	
				1^{--}	13434	12875	559	$\chi_{c0}(1P)Y(1S)$	
				2^{--}	13435	12971	464	$\chi_{c1}(1P)Y(1S)$	
		3S	0	0^{++}	13558	12383	1175	$\eta_c(1S)\eta_b(1S)$	
			1	1^{+-}	13566	12444	1122	$\eta_c(1S)Y(1S)$	
			2	2^{++}	13580	12557	1023	$J/\psi(1S)Y(1S)$	

From Tables 4-8 a number of conclusions can be drawn. First of all, with the exception of the two following states:

$$X_{bbbb} \quad 1D \quad S = 1 \quad 3^{+-} \quad 19720 \text{ MeV} \quad (37)$$

$$X_{bbbb} \quad 1D \quad S = 2 \quad 4^{++} \quad 19724 \text{ MeV}, \quad (38)$$

for all other tetraquark states there is at least one meson pair with the total mass less than the tetraquark mass ($\Delta_{\max} > 0$). Therefore for almost all tetraquarks there is a possibility of such fall-apart decay.

For most tetraquarks the value of Δ_{\max} significantly exceeds 300 MeV. These tetraquarks lie significantly higher than the decay thresholds and, thus, they rapidly fall-apart in the meson pair due to the quark and antiquark rearrangements. This means that experimentally such a state will manifest itself not as a narrow, but as a wide resonance which is hard to observe. However, such arguments can be applied only to the ground states of tetraquarks. For the excited states there are additional restrictions. In particular, these decays will be suppressed either by the centrifugal barrier between the quark and antiquark (for the orbital excitations), or by the zeros of the wave

Table 6. Same as in Table 4 but for the $cb\bar{c}\bar{b}$ states composed from the mixture of axialvector (A) and scalar (S) diquarks.

$QQ\bar{Q}\bar{Q}$	$d\bar{d}'$	State	S	J^{PC}	M	M_{thr}	Δ	Meson pair					
$cb\bar{c}\bar{b}$	$\frac{1}{\sqrt{2}}(A\bar{5} \pm S\bar{A})$	1S	1	1^{++}	12863	12557	306	$J/\psi(1S)Y(1S)$					
				1^{+-}		12444	419	$\eta_c(1S)Y(1S)$					
						12813	283	$\chi_{c0}(1P)\eta_b(1S)$					
				0^{-+}		12843	253	$\eta_c(1S)\chi_{b0}(1P)$					
						12986	110	$h_c(1P)Y(1S)$					
						12996	100	$J/\psi(1S)h_b(1P)$					
		1P	1	0^{--}	13096		12971	125	$\chi_{c1}(1P)Y(1S)$				
							12990	106	$J/\psi(1S)\chi_{b1}(1P)$				
							12877	222	$\eta_c(1S)\chi_{b1}(1P)$				
						1^{-+}	12909	190	$\chi_{c1}(1P)\eta_b(1S)$				
							12986	113	$h_c(1P)Y(1S)$				
							12996	103	$J/\psi(1S)h_b(1P)$				
				1^{--}	13099	1		12875	224	$\chi_{c0}(1P)Y(1S)$			
								12883	216	$\eta_c(1S)h_b(1P)$			
								12924	175	$h_c(1P)\eta_b(1S)$			
								12956	143	$J/\psi(1S)\chi_{b0}(1P)$			
								12971	128	$\chi_{c1}(1P)Y(1S)$			
								12990	109	$J/\psi(1S)\chi_{b1}(1P)$			
		2^{-+}	13104	1	1		13009	90	$J/\psi(1S)\chi_{b2}(1P)$				
							13016	83	$\chi_{c2}(1P)Y(1S)$				
							12896	208	$\eta_c(1S)\chi_{b2}(1P)$				
							12955	149	$\chi_{c2}(1P)\eta_b(1S)$				
							12986	118	$h_c(1P)Y(1S)$				
							12996	108	$J/\psi(1S)h_b(1P)$				
		2^{--}	13104	1	1		12971	133	$\chi_{c1}(1P)Y(1S)$				
							12990	114	$J/\psi(1S)\chi_{b1}(1P)$				
							13009	114	$J/\psi(1S)\chi_{b2}(1P)$				
							13016	114	$\chi_{c2}(1P)Y(1S)$				
						2S	13257	1	1	1^{++}	12557	700	$J/\psi(1S)Y(1S)$
										1^{+-}	12444	813	$\eta_c(1S)Y(1S)$
		1^{++}	12557	736	$J/\psi(1S)Y(1S)$								
		1D	13293	1	1	1^{+-}	12444	849	$\eta_c(1S)Y(1S)$				
						2^{++}	12557	741	$J/\psi(1S)Y(1S)$				
						2^{+-}	13298	13148	$\eta_c(1S)Y_2(1D)$				
							13222	76	$\psi_2(3823)\eta_b(1S)$				
							13261	44	$J/\psi(1S)Y_2(1D)$				
	13284					21	$\psi_2(3823)Y(1S)$						
2P	13305	1	1		13303	2	$\psi_3(3842)Y(1S)$						
					13241	64	$\psi_3(3842)\eta_b(1S)$						
				3^{+-}	13241	64	$\psi_3(3842)\eta_b(1S)$						
				0^{-+}	13426	12813	$\chi_{c0}(1P)\eta_b(1S)$						
				0^{--}	12971	455	$\chi_{c1}(1P)Y(1S)$						
				1^{-+}	13426	12877	$\eta_c(1S)\chi_{b1}(1P)$						
3S	13426	1	1	1^{--}	12875	549	$\eta_c(1S)\chi_{b1}(1P)$						
				1^{--}	12875	551	$\chi_{c0}(1P)Y(1S)$						
				2^{-+}	13427	12896	$\eta_c(1S)\chi_{b2}(1P)$						
				2^{--}	12971	456	$\chi_{c1}(1P)Y(1S)$						
3S	13566	1	1	1^{++}	12557	1009	$J/\psi(1S)Y(1S)$						
				1^{+-}	12444	1122	$\eta_c(1S)Y(1S)$						

Table 7. Same as in Table 4 but for the $cb\bar{c}\bar{b}$ states composed from the scalar (S) diquarks.

$QQ\bar{Q}\bar{Q}$	$d\bar{d}'$	State	S	J^{PC}	M	M_{thr}	Δ	Meson pair
$cb\bar{c}\bar{b}$	$S\bar{S}$	1S	0	0^{++}	12856	12383	473	$\eta_c(1S)\eta_b(1S)$
						12875	220	$\chi_{c0}(1P)Y(1S)$
		1P	0	1^{--}	13095	12883	212	$\eta_c(1S)h_b(1P)$
						12924	171	$h_c(1P)\eta_b(1S)$
						12956	139	$J/\psi(1S)\chi_{b0}(1P)$
						12971	124	$\chi_{c1}(1P)Y(1S)$
						12990	105	$J/\psi(1S)\chi_{b1}(1P)$
						13009	86	$J/\psi(1S)\chi_{b2}(1P)$
						13016	79	$\chi_{c2}(1P)Y(1S)$
						13250	867	$\eta_c(1S)\eta_b(1S)$
		1D	2^{++}	13293	12557	736	$J/\psi(1S)Y(1S)$	
		2P	1^{--}	13420	12875	545	$\chi_{c0}(1P)Y(1S)$	
		3S	0^{++}	13559	12383	1176	$\eta_c(1S)\eta_b(1S)$	

function (for the radial excitations), or both simultaneously, and therefore such tetraquark states can be observed as narrow resonances.

Next, there are also states for which $\Delta_{\text{max}} < 300$ MeV. Such states are close to the meson pair decay threshold and, thus, these fall-apart decays have a small phase. For such states, we show in Tables 4-8 not only Δ_{max} , but also all close-lying decay channels and their corresponding Δ in the range $-50 \leq \Delta \leq 300$ MeV. Small negative Δ are given because our calculations have a theoretical error. However, if the value of Δ_{max} is sufficiently negative, the state cannot decay via the strong fall-apart decay processes into two $Q\bar{Q}'$ quarkonia, and the main channels will be either a decay due to the heavy quark-antiquark annihilation into gluons with their subsequent hadronization into the lighter hadrons (strongly suppressed according to the Okubo-Zweig-Iizuka rule), or radiative decays (if allowed). As a result, this state will be a narrow state that can be observed experimentally in other decay channels: either to hadrons made up of lighter quarks and antiquarks, or two quarkonia and a photon.

All possible di- J/ψ and di- $Y(1S)$ decay thresholds are also given in Tables 4-8 (and highlighted in bold). Such decay channels are the most convenient for the experimental studies, since these mesons have a characteristic decay into a $\mu^+\mu^-$ pair with branching fractions $\sim 5\%$ and, thus, have a clear experimental signature.

So far, the results of experimental searches are fully correlated with our conclusions. In particular, the LHCb, CMS and ATLAS Collaborations are searching for the fully-charmed $cc\bar{c}\bar{c}$ and fully-bottom $bb\bar{b}\bar{b}$ tetraquarks. In Table 9 masses and widths of all currently observed fully-charmed tetraquark states and our candidates for the interpretation of such states are given. One state named X(6900) has already been reliably detected by all three Collaborations (LHCb 2020 [5], CMS 2022 [6], ATLAS 2022 [7]). It is clearly a candidate for the excited fully-charmed state. Moreover, the measured value of its mass is very close to our prediction. In fact we have 5 candidates for this resonance with the masses within the range of 50 MeV from the measured X(6900) mass. Thus it is important to measure the quantum numbers of this state (states?). Additionally LHCb data indicates two wide and not very distinctive peaks near 6.4 GeV and 7.2 GeV which can also be interpreted as ground and excited fully-charmed tetraquark states.

Very recently the CMS [6] and ATLAS [7] Collaborations reported preliminary results on the observation of exotic charmed states. The CMS Collaboration observed 3 distinct states in the $J/\psi J/\psi$ mass spectrum: X(6600), X(6900) and X(7300), while the ATLAS Collaboration observed 4 distinct states in the di- J/ψ and $J/\psi + \psi(2S)$ channels: X(6200), X(6600), X(6900) and X(7200). As it was already pointed out before, X(6900) is the most prominent of them all since it was observed by all three experiments with very close mass. The peaking structure around 7.2 GeV in LHCb data was confirmed in these experiments (X(7200) and X(7300)). The X(6200) observed by ATLAS is very close to our prediction for the lowest ground state 0^{++} with the mass 6190 MeV. The authors of Ref. [32] also predicted this state from the analysis of the LHCb data back in 2021. For the X(6600) structure observed both by CMS and ATLAS we also propose candidates but with greater deviations from central values of the observed mass.

Table 8. Same as in Table 4 but for the $bb\bar{b}\bar{b}$ states composed from the axialvector (A) diquarks.

$QQ\bar{Q}\bar{Q}$	$d\bar{d}'$	State	S	J^{PC}	M	M_{thr}	Δ	Meson pair			
$bb\bar{b}\bar{b}$	$A\bar{A}$	1S	0	0^{++}	19315	18798 18921	517 394	$\eta_b(1S)\eta_b(1S)$ Y(1S)Y(1S)			
			1	1^{+-}	19320	18859	461	$\eta_b(1S)Y(1S)$			
			2	2^{++}	19331	18921	410	Y(1S)Y(1S)			
		1P	0	1^{--}	19536	19298 19320 19353 19373	238 216 183 163	$\eta_b(1S)h_b(1P)$ Y(1S) $\chi_{b0}(1P)$ Y(1S) $\chi_{b1}(1P)$ Y(1S) $\chi_{b2}(1P)$			
					0^{-+}	19533	19258 19360	275 173	$\eta_b(1S)\chi_{b0}(1P)$ Y(1S) $h_b(1P)$		
						1^{-+}	19535	19291 19360	244 175	$\eta_b(1S)\chi_{b1}(1P)$ Y(1S) $h_b(1P)$	
					2^{-+}		19539	19311 19360	228 179	$\eta_b(1S)\chi_{b2}(1P)$ Y(1S) $h_b(1P)$	
			2	1^{--}		19534	19298 19320 19353 19373	236 214 181 161	$\eta_b(1S)h_b(1P)$ Y(1S) $\chi_{b0}(1P)$ Y(1S) $\chi_{b1}(1P)$ Y(1S) $\chi_{b2}(1P)$		
					2^{--}	19538	19353 19373	185 165	Y(1S) $\chi_{b1}(1P)$ Y(1S) $\chi_{b2}(1P)$		
						3^{--}	19545	19373	172	Y(1S) $\chi_{b2}(1P)$	
					2S	0	0^{++}	19680	18798 18921	882 759	$\eta_b(1S)\eta_b(1S)$ Y(1S)Y(1S)
			1	1^{+-}				19682	18859	823	$\eta_b(1S)Y(1S)$
			2	2^{++}				19687	18921	766	Y(1S)Y(1S)
			1D	0		2^{++}	19715	18921	794	Y(1S)Y(1S)	
							1^{+-}	19710	18859	851	$\eta_b(1S)Y(1S)$
		1^{+-}					19714	19562	152	$\eta_b(1S)Y_2(1D)$	
				3^{+-}		19720	19812	-92	$h_b(1P)\chi_{b2}(1P)$		
		2		0^{++}		19705	18798 18921	907 784	$\eta_b(1S)\eta_b(1S)$ Y(1S)Y(1S)		
						1^{++}	19707	18921	786	Y(1S)Y(1S)	
			19711	18921			790	Y(1S)Y(1S)			
			3^{++}	19717			19624	93	Y(1S) $Y_2(1D)$		
			4^{++}	19724			19824	-100	$\chi_{b2}(1P)\chi_{b2}(1P)$		
			2P	0		1^{--}	19820	19298	522	$\eta_b(1S)h_b(1P)$	
		0^{-+}					19821	19258	563	$\eta_b(1S)\chi_{b0}(1P)$	
							1^{-+}	19821	19291	530	$\eta_b(1S)\chi_{b1}(1P)$
		1		2^{-+}	19822	19311		511	$\eta_b(1S)\chi_{b2}(1P)$		
					1^{--}	19823	19298	525	$\eta_b(1S)h_b(1P)$		
						2^{--}	19823	19353	470	Y(1S) $\chi_{b1}(1P)$	
		2		3^{--}	19824		19373	451	Y(1S) $\chi_{b2}(1P)$		
					3S	0^{++}	19941	18798 18921	1143 1020	$\eta_b(1S)\eta_b(1S)$ Y(1S)Y(1S)	
1	1^{+-}						19943	18859	1084	$\eta_b(1S)Y(1S)$	
2	2^{++}	19947	18921	1026			Y(1S)Y(1S)				

On the other hand searches for the fully-bottom tetraquark in the process:

$$pp \longrightarrow X_{bb\bar{b}\bar{b}} \longrightarrow Y(1S)Y(1S) \quad (39)$$

in the mass range 17.5-20 GeV (covering the mass range we predict: 19.3-20 GeV) have not yet yielded any results (LHCb 2018 [10], CMS 2017 [11], 2020 [12]). Moreover, lattice calculations [33] do not find fully-bottom tetraquark bound states in this mass region. Such conclusion correlates with our results that the masses of the fully-bottom tetraquarks are significantly higher than the decay thresholds. Thus these states rapidly fall-apart and can appear only as wide, hard to detect resonances. However, according to our calculations, there are two states of such tetraquarks, corresponding to high orbital excitations with high values of total spin J , that lie below any decay thresholds, these are the states already mentioned in (37)-(38). Therefore, these states can be observed as narrow states decaying to lighter hadrons.

Table 9. Exotic X states observed by the LHCb [5], CMS [6] and ATLAS [7] Collaborations in di- J/ψ invariant mass spectra and our candidates. All masses are given in MeV.

Collaboration	State	Mass	Width	Our candidates			
				State	S	J^{PC}	Mass
ATLAS	X(6200)	$6220 \pm 50^{+40}_{-50}$	$310 \pm 120^{+70}_{-80}$	1S	0	0^{++}	6190
LHCb	X(6400)	≈ 6400		1S	2	2^{++}	6367
CMS	X(6600)	$6552 \pm 10 \pm 12$	$124 \pm 29 \pm 34$	1S	2	2^{++}	6367
ATLAS		$6620 \pm 30^{+20}_{-10}$	$310 \pm 90^{+60}_{-110}$	2S	0	0^{++}	6782
LHCb	X(6900)	$6905 \pm 11 \pm 7$	$80 \pm 19 \pm 33$	2S	2	2^{++}	6868
LHCb		$6886 \pm 11 \pm 11$	$168 \pm 33 \pm 69$	1D	0	2^{++}	6921
CMS		$6927 \pm 9 \pm 5$	$122 \pm 22 \pm 19$	1D	2	0^{++}	6899
ATLAS		$6870 \pm 30^{+60}_{-10}$	$120 \pm 40^{+30}_{-10}$	1D	2	2^{++}	6915
LHCb	X(7200)	≈ 7200		3S	0	0^{++}	7259
ATLAS		$7220 \pm 30^{+20}_{-30}$	$100^{+130+60}_{-70-50}$				
CMS	X(7300)	$7287 \pm 19 \pm 5$	$95 \pm 46 \pm 20$	3S	0	0^{++}	7259
				3S	2	2^{++}	7333

6. Theoretical predictions

In Tables 10-30 we compare our predictions for the masses (Table 3) with the results of other scientific groups obtained in different theoretical approaches.

We have introduced abbreviations in Tables 10-30, but only in cases when the authors used different models or parameter values within the same work. The most common abbreviations are the following.

- DA, MM, mix – diquark-antidiquark, meson-meson models and their mixing;
- (I-III) $_d$ – different sets of variable parameter values (quark masses, potential parameters, constants, etc.).

Other abbreviations that occur a few times only:

- SpB, OscI,II [34] – Spherical Bag Model and Oscillating Potential Model;
- QDCSM, ChQM [35] – Quark Delocalization Color Screening Model and Chiral Quark Model;
- RSM [36] – Real Scaling Method;
- Cur, Op [37,38] – different expressions for currents;
- LO, NLO, NLO \oplus G3 [37,39] – higher corrections;
- CQM, CMIM, MCFTM [40] – Constituent Quark Model, Color-Magnetic Interaction Model and Multiquark Color Flux-Tube Model;
- K [41,42] – other geometric configurations of the system that are neither diquark nor meson;
- NR, Rel [43] – non-relativistic and relativistic considerations, respectively;
- Bt, Fl [44] – “butterfly” and “flip-flop” potentials.

A few more clarifying notes to Tables 10-30:

- In many papers using the diquark-antidiquark picture, the cases of color antitriplet-diquark-triplet-antidiquark $\bar{3} \otimes 3$ and color sextet-diquark-antisextet-antidiquark $6 \otimes \bar{6}$ were considered. As we discussed in Sec. 2, in the color sextet (anti)diquark, the interaction potential

between (anti)quarks within the (anti)diquark is repulsive and thus corresponding diquark cannot be a bound state, which we consider inappropriate for our problem. Therefore, in Tables 10-30 we give theoretical predictions for the masses calculated only for the $\bar{3} \otimes 3$ configuration. If the results were a mixture of two configurations, we chose those masses that contain more of the triplet state in percentage. We note a general trend: in almost all cases, the calculated masses of sextet configurations turned out to be approximately 10 – 100 MeV higher than their triplet counterparts.

- In some papers (for example, [45]), tetraquarks containing excited diquarks were also considered. Again, as discussed in Sec. 2, we have limited ourselves to diquark ground states. Therefore, the masses of such tetraquarks, composed of excited diquarks, are not included in our comparison.
- *in [34] for model 1, corrections were calculated only for all 1S states and for the two lowest 1P states; corrections for all other states were not calculated.
- **Two cases were considered in [46]: the presence and absence of the heavy η_b -meson exchange. The results only for the case without such an exchange are given.
- ***in [37], LO results were also obtained, but they are quite similar to NLO \oplus G3, so we do not present them.
- ****in [39], all results were obtained in two mass schemes: in the \overline{MS} -scheme and on-Shell-scheme. In view of the already colossal number of results of this study, we took the masses only in the \overline{MS} -scheme.

Table 10. Comparison of theoretical predictions for the masses of the $cc\bar{c}\bar{c}$ tetraquark ground state (1S) with the axialvector diquark and antidiquark. S is the total spin of the diquark-antidiquark system. All masses are given in MeV. Masses are sorted chronologically, oldest predictions first.

$d\bar{d}'$ State S J^{PC}	$A\bar{A}$		
	1S		
	0 0^{++}	1 1^{+-}	2 2^{++}
Our	6190	6271	6367
[47]	6200		
	6276 (DA, SpB);	6276 (DA, SpB);	6276 (DA, SpB);
[34]*	6426 (DA, OscI);	6440 (DA, OscI);	6469 (DA, OscI);
	6450 (DA, OscII);	6450 (DA, OscII);	6450 (DA, OscII);
	6221, 6260 (MM, SpB)	6221, 6260 (MM, SpB)	6221, 6260 (MM, SpB)
[48]	6477	6528	6573
[49]	6038 ÷ 6115	6101 ÷ 6176	6172 ÷ 6216
[50]	5970	6050	6220
[51]	5966	6051	6223
[52]	5300 ± 500		
[53]	6192 ± 25		
[54]	5990 ± 80		6090 ± 80
[55], [56]	6460 ± 160, 6470 ± 160	6510 ± 150	6510 ± 150
[57]	7016	6899	6956
[43]	≲ 6140		
[58], [59]	5969	6021	6115
[60]	6487	6500	6524
[61]	5970 ± 40		
[62]		6050 ± 80	
[63]	6425 (Id); 6483 (IIId)	6425 (Id); 6450 (IIId)	6432 (Id); 6479 (IIId)
[64]	5883	6120	6246
[65]	6192 ± 25		6429 ± 25

Table 10. Table continued.

$d\bar{d}'$ State S J^{PC}	$A\bar{A}$		
	1S		
	0	1	2
	0^{++}	1^{+-}	2^{++}
Our	6190	6271	6367
	6128, 6270,	6149, 6285,	6197, 6314,
	6358 (DA, QDCSM (I-III) _d);	6375 (DA, QDCSM (I-III) _d);	6407 (DA, QDCSM (I-III) _d);
[35]	6466, 6482,	6479, 6488,	6498, 6499,
	6493 (DA, ChQM (I-III) _d);	6495 (DA, ChQM (I-III) _d);	6505 (DA, ChQM (I-III) _d);
	5961 ÷ 6206 (MM, QDCSM (I-III) _d);	6079 ÷ 6088 (MM, QDCSM (I-III) _d);	6197 ÷ 6207 (MM, QDCSM (I-III) _d);
[66]	5961 ÷ 6701 (MM, ChQM (I-III) _d)	6079 ÷ 6575 (MM, ChQM (I-III) _d)	6197 ÷ 6602 (MM, ChQM (I-III) _d)
[45]	6542	6515	6543
	6455	6500	6524
	6360 (DA);	6398 (DA);	6410 (DA);
[36]	5973 (MM);	6084 (MM);	6194 (MM);
	5973 (mix);	6084 (mix);	6194 (mix);
	6510 (RSM)	6600 (RSM)	6708 (RSM)
[67]	5960 (Id);	6009 (Id);	6100 (Id);
	6198 (IIId)	6246 (IIId)	6323 (IIId)
	6450 ± 75 (DA, Cur, NLO \oplus G3);		
[37]***, [38]	6471 ± 67 (DA, Op, NLO \oplus G3);		
	6029 ± 198, 6376 ± 367,		
	6494 ± 66, 6675 ± 98 (MM)		
	6469 (DA);	6674 (DA);	7026 (DA);
[68]	6536, 6657 (MM);	6671 (MM);	7030 (MM);
	6423, 6650 (mix)	6627 (mix)	7014 (mix)
[69]	6351	6441	6471
[70]	6476	6441	6475
	6573 (CQM);	6580 (CQM);	6607 (CQM);
[40]	6035 (CMIM);	6139 (CMIM);	6194 (CMIM);
	6454 (MCFTM)	6463 (MCFTM)	6486 (MCFTM)
[71]	6460^{+130}_{-170}		
[72]	6200		
[73]	6520 ± 100	6570 ± 100	6600 ± 100
	6419 (Id);	6456 (Id);	6516 (Id);
[74]	6390 (IIId);	6419 (IIId);	6476 (IIId);
	6415 (IIIId)	6454 (IIIId)	6514 (IIIId)
[75]	6196		
[76]	6440 ± 110, 6520 ± 110,	-	
	6870 ± 110, 6960 ± 110		
[77]	6271	6231	6287
	6421 (DA);	6439 (DA);	6472 (DA);
[41], [42]	5936, 6268 (MM);	6070, 6325 (MM);	6204, 6338 (MM);
	6150, 6340 (K)	6271, 6436 (K)	6358, 6473 (K)
[78]	5939	5986	6079
[79]	6498	6481	6502
[80]	6466	6494	6551
[81]	6906	5955 (Id);	5960
		6896 (IIId)	
[82]	6322	6354	6385
[83]	6360^{+180}_{-160} , 6540^{+190}_{-180}	6470^{+180}_{-170}	6520^{+170}_{-170}
	6270 (Id);	6424 (Id);	6424 (Id);
[84]	6271 (IIId);	6435 (IIId);	6435 (IIId);
	6201 (IIIId)	6396 (IIIId)	6391 (IIIId)
[85]	6055^{+69}_{-74}		6090^{+62}_{-66}
[86]	7438-7542		

Table 10. Table continued.

$d\bar{d}'$ State S J^{PC}	$A\bar{A}$		
	1S		
	0	1	2
	0^{++}	1^{+-}	2^{++}
Our	6190	6271	6367
[44]	6874 (Bt); 6850 (FL); 6822 (mix)	6913 (Bt); 6870 (FL); 6822 (mix)	6990 (Bt); 6913 (FL); 6822 (mix)
[87]	5978	6155	6263
[39]****	6070^{+50}_{-70} , 6070^{+80}_{-100} (DA, LO); 6600^{+90}_{-100} , 6690^{+100}_{-120} (DA, NLO); $5090^{+60}_{-80} \div 7110^{+130}_{-150}$ (MM, LO); $6360^{+60}_{-100} \div 8330^{+130}_{-150}$ (MM, NLO)	6080^{+40}_{-100} (DA, LO); 6650^{+100}_{-130} (DA, NLO); $6040^{+60}_{-80} \div 7070^{+140}_{-160}$ (MM, LO); $6650^{+90}_{-100} \div 8320^{+180}_{-200}$ (MM, NLO)	6070^{+80}_{-100} , 6150^{+80}_{-100} (DA, LO); 6980^{+90}_{-110} , 7250^{+100}_{-110} (DA, NLO); $6110^{+60}_{-80} \div 7100^{+130}_{-150}$ (MM, LO); $7030^{+100}_{-120} \div 8890^{+210}_{-240}$ (MM, NLO)
[88]	6200 ± 100	6240 ± 100	6270 ± 90
[89]	7035, 7202	7050, 7274	7069, 7281
[90]	6384	6452	6483
[91]	6035	6137	6194

Table 11. Same as in Table 10 but for the first orbital excitation (1P).

$d\bar{d}'$ State S J^{PC}	$A\bar{A}$						
	1P						
	0	1			2		
	1^{--}	0^{-+}	1^{-+}	2^{-+}	1^{--}	2^{--}	3^{--}
Our	6631	6628	6634	6644	6635	6648	6664
[92]	6550	6550	6550	6550	6550	6550	6550
[34]*	6694 (OscI); 6714 (OscII)	6695 (OscI); 6714 (OscII)	6718 (OscI); 6714 (OscII)	6718 (OscI); 6714 (OscII)	6718 (OscI); 6714 (OscII)	6718 (OscI); 6714 (OscII)	6718 (OscI); 6714 (OscII)
[48]	7004	6969	7013	7033			
[49]	$6998 \div 7052$	$6993 \div 7051$	$7275 \div 7363$	$7002 \div 7055$		$7278 \div 7357$	
[93]	6420^{+29}_{-32} (DA); 6411^{+25}_{-43} (MM)						
[55], [56]	6830 ± 180	6850 ± 180	6880 ± 180				
[58], [59]	6577	6480	6577	6610	6495	6600	6641
[62]	6110 ± 80						
[64]	6580	6596			6584		
[45]	6636	6681	6676	6667	6768	6630	6801
[78]	6553	6460	6554	6587	6459	6577	6623
[79]	6740	6723	6743	6752	6740	6739	6753
[81]	6060 (Id); 6999 (IIId)	6054 (Id); 6995 (IIId)	6054 (Id); 6995 (IIId)	6054 (Id); 6995 (IIId)	6056 (Id); 6996 (IIId)	6056 (Id); 6996 (IIId)	6056 (Id); 6996 (IIId)
[83]	6990^{+230}_{-200} , 7170^{+280}_{-220} , 6610^{+120}_{-150}	7000^{+230}_{-200} , 7020^{+240}_{-200} , 6540^{+120}_{-140}	6980^{+210}_{-190} , 7070^{+210}_{-190} , 6530^{+110}_{-160}				
[39]****	(DA, LO); 7970^{+100}_{-170} (DA, NLO); 6530^{+110}_{-140} $\div 6610^{+120}_{-140}$ (MM, LO); 7550^{+140}_{-150} $\div 8090^{+60}_{-160}$ (MM, NLO)	(DA, LO); 7510^{+120}_{-160} (DA, NLO); 6530^{+120}_{-140} $\div 6560^{+120}_{-150}$ (MM, LO); 7300^{+110}_{-130} $\div 8530^{+150}_{-190}$ (MM, NLO)	(DA, LO); 8020^{+80}_{-170} (DA, NLO); 6530^{+110}_{-140} $\div 6610^{+120}_{-140}$ (MM, LO); 7550^{+140}_{-150} $\div 8090^{+60}_{-160}$ (MM, NLO)				
[88]	6330 ± 100						

Table 12. Same as in Table 10 but for the first radial excitation (2S).

$d\bar{d}'$ State S J^PC	$A\bar{A}$		
	2S		
	0	1	2
	0^{++}	1^{+-}	2^{++}
Our	6782	6816	6868
[58], [59]	6663	6675	6698
[63]		6856 (Id); 6894 (IIId)	6864 (Id); 6919 (IIId)
[64]	6573	6669	6739
[65]	6871 ± 25		6967 ± 25
[35]	6950, 6975 (DA, QDCSM (I-III) _d); 6825, 6900, 6910 (DA, ChQM (I-III) _d)	7250, 7280 (DA, QDCSM (I-III) _d); 7250, 7275, 7280 (DA, ChQM (I-III) _d)	
[66]	6940	6928	6948
[70]	6908	6896	6921
[94]	6480 ± 80	6520 ± 80	6560 ± 80
[74]	6916 (Id); 6773 (IIId); 6924 (IIIId)	6957 (Id); 6792 (IIId); 6966 (IIIId)	7001 (Id); 6843 (IIId); 7011 (IIIId)
[78]	6642	6654	6676
[79]	7007	6954	6917
[80]	6883	6911	6968
[81]	7073 (Id); 8095 (IIId)	7025 (Id); 8060 (IIId)	7041 (Id); 8072 (IIId)
[82]	6575	6609	6639
[84]	6393 (Id); 6411 (IIId); 6575 (IIIId)	6458 (Id); 6502 (IIId); 6799 (IIIId)	6458 (Id); 6502 (IIId); 6794 (IIIId)
[85]	6555^{+36}_{-37}		6566^{+34}_{-35}
[95]	6908	6919	6927
[88]	6570 ± 90	6640 ± 90	6690 ± 90

Table 13. Same as in Table 10 but for the second orbital excitation (1D).

$d\bar{d}'$ State S J^{PC}	$A\bar{A}$								
	1D								
	0			1			2		
	2^{++}	1^{+-}	2^{+-}	3^{+-}	0^{++}	1^{++}	2^{++}	3^{++}	4^{++}
Our	6921	6909	6920	6932	6899	6904	6915	6929	6945
[92]	6780	6780	6780	6780	6780	6780	6780	6780	6780
[49]			6586 ÷ 6648			6530 ÷ 6609			
[55], [56]						6340 ± 190			
[64]	6827	6829			6827	6827	6827		
[35]					7140, 7150, 7170 (DA, QDCSM (I-III) _d); 7150, 7160 (DA, ChQM (I-III) _d)				
[95]	6832	6833	6835	6844	6848	6851	6857	6863	6870
[39]****						7040 ⁺¹³⁰ ₋₁₅₀ (DA, LO); 7410 ⁺²³⁰ ₋₃₀₀ (DA, NLO); 6040 ⁺⁶⁰ ₋₈₀ ÷ 7070 ⁺¹⁴⁰ ₋₁₆₀ (MM, LO); 6650 ⁺⁹⁰ ₋₁₀₀ ÷ 8320 ⁺¹⁸⁰ ₋₂₀₀ (MM, NLO)			

Table 14. Same as in Table 10 but for the first orbital and radial excitation (2P).

$d\bar{d}'$ State S J^{PC}	$A\bar{A}$							
	2P							
	0		1			2		
	1^{--}	0^{-+}	1^{-+}	2^{-+}	1^{--}	2^{--}	3^{--}	
Our	7091	7100	7099	7098	7113	7113	7112	
[58], [59]	6944	6867	6944	6970	6876	6962	6997	
[64]	6940	6953			6943			
[94]	6580 ± 90							
[78]	6925	6851	6926	6951	6849	6944	6982	
[81]	7143 (I _d); 8174 (II _d)	7130 (I _d); 8162 (II _d)	7130 (I _d); 8162 (II _d)	7130 (I _d); 8162 (II _d)	7134 (I _d); 8166 (II _d)	7134 (I _d); 8166 (II _d)	7134 (I _d); 8166 (II _d)	
[88]	6740 ± 90							

Table 15. Same as in Table 10 but for the second radial excitation (3S).

$d\bar{d}'$ State S J^{PC}	$A\bar{A}$		
	3S		
	0	1	2
	0^{++}	1^{+-}	2^{++}
Our	7259	7287	7333
[63]		6915 (Id); 7036 (IIId)	6919 (Id); 7058 (IIId)
[64]	6948	7016	7071
[35]	7225, 7250 (DA, QDCSM (I-III) _d); 7210, 7250, 7260 (DA, ChQM (I-III) _d)		
[66]	7063	7052	7064
[70]	7296	7300	7320
[94]	6940 ± 80	6960 ± 80	7000 ± 80
[74]	7224 (Id); 7054 (IIId); 7229 (IIIId)	7263 (Id); 7066 (IIId); 7268 (IIIId)	7257 (Id); 7097 (IIId); 7258 (IIIId)
[78]	7010	7017	7032
[79]		7024	7030
[80]	7225	7253	7310
[82]	6782	6814	6842
[84]	6441 (Id); 6477 (IIId); 6897 (IIIId)	6464 (Id); 6536 (IIId); 7148 (IIIId)	6464 (Id); 6536 (IIId); 7148 (IIIId)
[85]	6883^{+27}_{-27}		6890^{+27}_{-26}
[95]	7240	7243	7248
[88]	6920 ± 90	7030 ± 90	7090 ± 90

Table 16. Same as in Table 10 but for the ground state (1S) of $cb\bar{c}\bar{b}$ composed from the axialvector diquark and antidiquark.

$d\bar{d}'$ State S J^{PC}	$A\bar{A}$		
	1S		
	0 0^{++}	1 1^{+-}	2 2^{++}
Our	12838	12855	12883
[51]	12471	12488	12566
[57]	13483	13592	13590
[43]	$\lesssim 12620$		
[60]	12864	12864	12884
[96]	12746 (DA); 12322, 12684 (MM); 12322 (mix)	12776 (DA); 12432, 12737 (MM); 12432 (mix)	12809 (DA); 12561, 12791 (MM); 12561 (mix)
[64]	12374	12491	12576
[69]	12534	12510	12582
[40]	13043 (CQM); 12354 (CMIM); 12955 (MCFTM)	13052 (CQM); 12436 (CMIM); 12955 (MCFTM)	13084 (CQM); 12548 (CMIM); 12984 (MCFTM)
[76]	$12510 \pm 100, 12580 \pm 100,$ $12670 \pm 100, 12740 \pm 110$	-	
[77]	12682	12720	12755
[41], [42]	12861 (DA); 12369, 12809 (MM); 12599, 12717 (K)	12888 (DA); 12431, 12843 (MM); 12635, 12768 (K)	12926 (DA); 12565, 12885 (MM); 12771, 12844 (K)
[97]	12460^{+170}_{-150}	12380^{+130}_{-120}	12300^{+150}_{-140}
[85]	12387^{+109}_{-120}		12401^{+117}_{-106}
[87]	12503	12016	12897
[90]	12759	12797	12882
[91]	12595	12573	12597

Table 17. Same as in Table 10 but for the first orbital excitation (1P) of $cb\bar{c}\bar{b}$ composed from the axialvector diquark and antidiquark.

$d\bar{d}'$ State S J^{PC}	$A\bar{A}$						
	1P						
	0		1		2		
	1^{--}	0^{-+}	1^{+-}	2^{-+}	1^{--}	2^{--}	3^{--}
Our	13103	13100	13103	13108	13103	13109	13116
[64]	12934	12943			12944		

Table 18. Same as in Table 10 but for the first radial excitation (2S) of $cb\bar{c}\bar{b}$ composed from the axialvector diquark and antidiquark.

$d\bar{d}'$ State S J^{PC}	$A\bar{A}$		
	2S		
	0 0^{++}	1 1^{+-}	2 2^{++}
Our	13247	13256	13272
[64]	12975	13022	13063
[85]	12911^{+48}_{-51}		12914^{+49}_{-49}

Table 19. Same as in Table 10 but for the second orbital excitation (1D) of $cb\bar{c}\bar{b}$ composed from the axialvector diquark and antidiquark.

$d\bar{d}'$ State S J^{PC}	$A\bar{A}$								
	1D								
	0	1			2				
	2^{++}	1^{+-}	2^{+-}	3^{+-}	0^{++}	1^{++}	2^{++}	3^{++}	4^{++}
Our	13306	13299	13304	13311	13293	13296	13301	13308	13317
[64]	13166	13167			13170	13168	13166		

Table 20. Same as in Table 10 but for the first orbital and radial excitation (2P) of $cb\bar{c}\bar{b}$ composed from the axialvector diquark and antidiquark.

$d\bar{d}'$ State S J^{PC}	$A\bar{A}$						
	2P						
	0	1			2		
	1^{--}	0^{-+}	1^{-+}	2^{-+}	1^{--}	2^{--}	3^{--}
Our	13428	13431	13431	13431	13434	13435	13436
[64]	13262	13269			13269		

Table 21. Same as in Table 10 but for the second radial excitation (3S) of $cb\bar{c}\bar{b}$ composed from the axialvector diquark and antidiquark.

$d\bar{d}'$ State S J^{PC}	$A\bar{A}$		
	3S		
	0	1	2
	0^{++}	1^{+-}	2^{++}
Our	13558	13566	13580
[64]	13301	13335	13365
[85]	13200^{+35}_{-36}		13202^{+35}_{-36}

Table 22. Same as in Table 10 but for the ground state (1S) first orbital excitation (1P) and first radial excitation (2S) of $cb\bar{c}\bar{b}$ composed from the mixture of axialvector and scalar diquark and antiquark.

$d\bar{d}'$	$\frac{1}{\sqrt{2}}(A\bar{S} \pm S\bar{A})$				
	1S		1P		2S
	1				
	$1^{+\pm}$	$0^{-\pm}$	$1^{-\pm}$	$2^{-\pm}$	$1^{+\pm}$
Our	12863	13096	13099	13104	13257
[51]	12485 (+); 12424 (-)				
[57]	13599 (+); 13555 (-)				
[60]	12870 (+); 12852 (-)				
[96]	12804 (DA); 12561, 12737 (MM); 12561 (mix) (+)				
[64]	12533	12922	12922 (-)		13036
[69]	12569 (+); 12510 (-)				
[77]	12703 (+); 12744 (-)				
[41], [42]	12903 (DA); 12431, 12843 (MM); 12635, 12768 (K) (+)				
[97]	12300^{+150}_{-140} (+); 12320^{+150}_{-130} (-)				
[87]	12155 (+); 12896 (-)				
[90]	12857 (+)				
[91]	12538 (+); 12339 (-)				

Table 23. Same as in Table 10 but for the second orbital excitation (1D) first orbital and radial excitation (2P) and second radial excitation(3S) of $cb\bar{c}\bar{b}$ composed from the mixture of axialvector and scalar diquark and antiquark.

$d\bar{d}'$	$\frac{1}{\sqrt{2}}(A\bar{S} \pm S\bar{A})$						
	1D			2P			3S
	1						
	$1^{+\pm}$	$2^{+\pm}$	$3^{+\pm}$	$0^{-\pm}$	$1^{-\pm}$	$2^{-\pm}$	$1^{+\pm}$
Our	13293	13298	13305	13426	13426	13427	13566
[64]	13154			13250	13250 (-)		13342

Table 24. Same as in Table 10 but for the ground state (1S), first orbital excitation (1P), first radial excitation (2S), second orbital excitation (1D), first orbital and radial excitation (2P), second radial excitation (3S) of $cb\bar{c}b$ composed from the scalar diquark and antidiquark.

$d\bar{d}'$ State S J^{PC}	$S\bar{S}$					
	1S	1P	2S	1D	2P	3S
	0					
	0^{++}	1^{--}	0^{++}	2^{++}	1^{--}	0^{++}
Our	12856	13095	13250	13293	13420	13559
[51]	12359					
[57]	13553					
[60]	12835					
[64]	12521	12910	13024	13143	13238	13330
[69]	12534					
[77]	12747					
[41], [42]	12892 (DA); 12369, 12809 (MM); 12599, 12717 (K)					
[97]	12280^{+150}_{-140}					
[87]	12359					
[91]	12431					

Table 25. Same as in Table 10 but for the ground state (1S) of the $bb\bar{b}\bar{b}$.

$d\bar{d}'$ State S J^{PC}	$A\bar{A}$		
	1S		
	0	1	2
	0^{++}	1^{+-}	2^{++}
Our	19315	19320	19331
[51]	18754	18808	18916
[53]	18826 ± 25		
[54]	18840 ± 90		18850 ± 90
[55], [56]	18460 ± 140 , 18490 ± 160	18540 ± 150	18530 ± 150
[98]	18800		
[57]	20275	20212	20243
[43]	18720 ± 20 (NR, MM); 18750 ± 50 (Rel, DA); $\lesssim 18890$		
[33]	> 18798	> 18859	> 18921
[60]	19322	19329	19341
[46]**	19191, 19221 (DA); 18670, 18928, 19195, 19205 (MM); 18670 (mix)	19227 (DA); 18799, 19179 (MM); 18799 (mix)	19238 (DA); 18928, 19195 (MM); 18928 (mix)
[61]	18690 ± 30		
[62]		18840 ± 90	
[63]	19247 (Id); 19305 (IIId)	19247 (Id); 19311 (IIId)	19249 (Id); 19325 (IIId)
[64]	18748	18828	18900
[65]	18826 ± 25		18956 ± 25

Table 25. Table continued.

$d\bar{d}'$ State S J^{PC}	$A\bar{A}$		
	1S		
	0	1	2
	0^{++}	1^{+-}	2^{++}
Our	19315	19320	19331
	19165, 19256, 19344 (DA, QDCSM (I-III) _d);	19184, 19264, 19354 (DA, QDCSM (I-III) _d);	19236, 19279, 19374 (DA, QDCSM (I-III) _d);
[35]	19313, 19456, 19466 (DA, ChQM (I-III) _d); 18800 ÷ 18925 (MM, QDCSM (I-III) _d); 18800 ÷ 20041 (MM, ChQM (I-III) _d)	19323, 19461, 19467 (DA, ChQM (I-III) _d); 18860 ÷ 18864 (MM, QDCSM (I-III) _d); 18860 ÷ 19927 (MM, ChQM (I-III) _d)	19344, 19471 (DA, ChQM (I-III) _d); 18921 ÷ 18925 (MM, QDCSM (I-III) _d); 18921 ÷ 19933 (MM, ChQM (I-III) _d)
[66]	19255	19251	19262
[45]	19306	19329	19341
[67]	18723 (Id); 18754 (II d)	18738 (Id); 18768 (II d)	18768 (Id); 18797 (II d)
[37]***, [38]	19872 ± 156 (DA, Cur, NLO ⊕ G3); 19717 ± 118 (DA, Op, NLO ⊕ G3); 19259 ± 88, 19430 ± 145, 19770 ± 137, 19653 ± 131 (MM)		
[68]	17975, 19033 (DA); 17999, 18038, 19036, 19069 (MM); 17917, 18010, 19280 (mix)	18065, 19093 (DA); 18062, 19087 (MM); 18009, 19338, 19627 (mix)	18241, 19211 (DA); 18238, 19207 (MM); 18189, 19451, 19708 (mix)
[69]	19199	19276	19289
[70]	19226	19214	19232
[40]	19417 (CQM); 18834 (CMIM); 19377 (MCFTM)	19413 (CQM); 18890 (CMIM); 19373 (MCFTM)	19429 (CQM); 18921 (CMIM); 19387 (MCFTM)
[99]	19650, 20110, 21470 (Id); 22310, 22660, 23720 (II d)		
[74]	19205 (Id); 19187 (II d); 19209 (III d)	19221 (Id); 19202 (II d); 19225 (III d)	19253 (Id); 19234 (II d); 19257 (III d)
[75]	18572		
[76]	18380 ± 110, 18440 ± 100, 18500 ± 100, 18590 ± 110	-	
[77]	18981	18969	19000
[41], [42]	19196 (DA); 18802, 19144 (MM); 18977, 19143 (K)	19205 (DA); 18864, 19126 (MM); 19053, 19206 (K)	19223 (DA); 18926, 19197 (MM); 19093, 19225 (K)
[100]	18719 (Id); 18749 (II d)	18734 (Id); 18764 (II d)	18764 (Id); 18792 (II d)
[82]	19666	19673	19680
[83]	18130 ⁺¹³⁰ ₋₉₀ , 18150 ⁺¹⁴⁰ ₋₁₀₀	18140 ⁺¹⁴⁰ ₋₉₀	18150 ⁺¹⁴⁰ ₋₁₉₀
[84]	19429 (Id); 19428 (II d); 19302 (III d)	19557 (Id); 19558 (II d); 19409 (III d)	19557 (Id); 19558 (II d); 19409 (III d)
[85]	18475 ⁺¹⁵¹ ₋₁₆₉ 18444 (Bt);	18444 (Bt);	18483 ⁺¹⁴⁹ ₋₁₆₈ 18444 (Bt);
[44]	18440 (FL); 18440 (mix)	18440 (FL); 18440 (mix)	18440 (FL); 18440 (mix)

Table 25. Table continued.

$d\bar{d}'$ State S J^{PC}	$A\bar{A}$		
	1S		
	0	1	2
	0^{++}	1^{+-}	2^{++}
Our	19315	19320	19331
[87]	18752	18805	18920
	18500^{+170}_{-260} , 18510^{+170}_{-260}	18500^{+170}_{-250}	18500^{+170}_{-260}
	(DA, LO);	(DA, LO);	(DA, LO);
	18970^{+50}_{-110}	18970^{+60}_{-110}	18910^{+110}_{-180} , 18950^{+70}_{-130}
	(DA, NLO);	(DA, NLO);	(DA, NLO);
[39]****	$18500^{+170}_{-260} \div 19210^{+200}_{-260}$	$18500^{+170}_{-260} \div 19210^{+200}_{-260}$	$18500^{+170}_{-260} \div 19210^{+200}_{-260}$
	(MM, LO);	(MM, LO);	(MM, LO);
	$18930^{+90}_{-160} \div 19660^{+50}_{-100}$	$18600^{+190}_{-260} \div 19530^{+110}_{-170}$	$18890^{+110}_{-180} \div 19620^{+40}_{-80}$
	(MM, NLO)	(MM, NLO)	(MM, NLO)
[90]	19240	19304	19328
[91]	18834	18890	18921

Table 26. Same as in Table 10 but for the first orbital excitation (1P) of the $b\bar{b}\bar{b}$.

$d\bar{d}'$ State S J^{PC}	$A\bar{A}$						
	1P						
	0	1			2		
	1^{--}	0^{-+}	1^{-+}	2^{-+}	1^{--}	2^{--}	3^{--}
Our	19536	19533	19535	19539	19534	19538	19545
[55], [56]	18770 ± 160	18790 ± 180	18830 ± 180				
[62]	18890 ± 90						
[64]	19281	19288			19288		
[45]	19479	19500	19496	19492	19603	19476	19617
[100]	19381 (Id); 19361 (IIId)	19340 (Id); 19327 (IIId)	19380 (Id); 19361 (IIId)	19395 (Id); 19373 (IIId)	19338 (Id); 19325 (IIId)	19390 (Id); 19369 (IIId)	19412 (Id); 19388 (IIId)
[83]	18460^{+150}_{-110}	18450^{+150}_{-110} , 18540^{+160}_{-120}	18560^{+160}_{-110} , 18790^{+180}_{-130}				
	18860^{+190}_{-260}	18860^{+190}_{-240}	18860^{+190}_{-260}				
	(DA, LO);	(DA, LO);	(DA, LO);				
[39]****	19180^{+130}_{-200}	19230^{+80}_{-140}	19230^{+70}_{-130}				
	(DA, NLO);	(DA, NLO);	(DA, NLO);				
	18850^{+200}_{-260}	18850^{+190}_{-260}	18850^{+200}_{-260}				
	$\div 18870^{+190}_{-260}$	$\div 18860^{+190}_{-260}$	$\div 18870^{+190}_{-260}$				
	(MM, LO);	(MM, LO);	(MM, LO);				
	19220^{+50}_{-110}	19180^{+110}_{-180}	19220^{+50}_{-110}				
	$\div 19310^{+40}_{-90}$	$\div 19310^{+40}_{-90}$	$\div 19310^{+40}_{-90}$				
	(MM, NLO)	(MM, NLO)	(MM, NLO)				

Table 27. Same as in Table 10 but for the first radial excitation (2S) of the $bb\bar{b}\bar{b}$.

$d\bar{d}'$ State S J^{PC}	$A\bar{A}$		
	2S		
	0	1	2
	0^{++}	1^{+-}	2^{++}
Our	19680	19682	19687
[63]		19594 (Id); 19813 (IIId)	19596 (Id); 19823 (IIId)
[64]	19335	19366	19398
[65]	19434 \pm 25		19481 \pm 25
[66]	19625	19625	19633
[70]	19583	19582	19594
[74]	19636 (Id); 19544 (IIId); 19646 (IIIId)	19662 (Id); 19565 (IIId); 19671 (IIIId)	19684 (Id); 19591 (IIId); 19694 (IIIId)
[100]	19441 (Id); 19414 (IIId)	19443 (Id); 19416 (IIId)	19448 (Id); 19421 (IIId)
[82]	19841	19849	19855
[84]	19512 (Id); 19515 (IIId); 19591 (IIIId)	19587 (Id); 19597 (IIId); 19728 (IIIId)	19587 (Id); 19597 (IIId); 19728 (IIIId)
[85]	19073 ⁺⁵⁹ ₋₆₃		19075 ⁺⁵⁹ ₋₆₂
[95]	19719	19722	19726

Table 28. Same as in Table 10 but for the second orbital excitation (1D) of the $bb\bar{b}\bar{b}$.

$d\bar{d}'$ State S J^{PC}	$A\bar{A}$									
	1D									
	0		1			2				
	2^{++}	1^{+-}	2^{+-}	3^{+-}	0^{++}	1^{++}	2^{++}	3^{++}	4^{++}	
Our	19715	19710	19714	19720	19705	19707	19711	19717	19724	
[55], [56]						18320 \pm 180				
[64]	19510	19511			19513	19512	19510			
[95]	19669	19671	19672	19675	19677	19678	19680	19684	19686	
[39]****						19200 ⁺²⁰⁰ ₋₂₆₀ (DA, LO); 18850 ⁺¹⁹⁰ ₋₂₆₀ (DA, NLO); 18500 ⁺¹⁷⁰ ₋₂₆₀ \div 19210 ⁺²⁰⁰ ₋₂₆₀ (MM, LO); 18600 ⁺¹⁹⁰ ₋₂₆₀ \div 19530 ⁺¹¹⁰ ₋₁₇₀ (MM, NLO)				

Table 29. Same as in Table 10 but for the second orbital and radial excitation (2P) of the $b\bar{b}\bar{b}\bar{b}$.

d \bar{d} ' State S J ^{PC}	A \bar{A}						
	2P						
	0		1		2		
	1 ⁻⁻	0 ⁻⁺	1 ⁻⁺	2 ⁻⁺	1 ⁻⁻	2 ⁻⁻	3 ⁻⁻
Our [64]	19820 19597	19821 19602	19821	19822	19823 19602	19823	19824

Table 30. Same as in Table 10 but for the third radial excitation (3S) of the $b\bar{b}\bar{b}\bar{b}$.

d \bar{d} ' State S J ^{PC}	A \bar{A}		
	3S		
	0	1	2
	0 ⁺⁺	1 ⁺⁻	2 ⁺⁺
Our [63]	19941	19943	19947
[64]	19644	19665	19688
[66]	19726	19733	19736
[70]	19887	19889	19898
[74]	19907 (Id); 19795 (IIId); 19913 (IIIId)	19930 (Id); 19815(IIId); 19936 (IIIId)	19926 (Id); 19822 (IIId); 19930 (IIIId)
[100]	19759 (Id); 19701 (IIId)	19760 (Id); 19703 (IIId)	19764 (Id); 19706 (IIId)
[82]	20001	20012	20021
[84]	19557 (Id); 19565 (IIId); 19845 (IIIId)	19597 (Id); 19615 (IIId); 20016 (IIIId)	19597 (Id); 19615 (IIId); 20016 (IIIId)
[85]	19353 ⁺⁴² ₋₄₂		19355 ⁺⁴¹ ₋₄₃
[95]	19979	19980	19982

We compare our predictions with the results obtained in the following approaches and models:

- Various quark models: [34–36,40–53,57–61,63–70,72,74,75,77–82,84–87,89–92,95,96,98–100].
- QCD sum rules: [37–39,54–56,62,71,73,76,83,88,94,97].
- Lattice calculations: [33,93].

Among them the following configurations can be distinguished:

- Diquark-antidiquark model: [33–37,39–46,50,51,53–69,71,73–75,77–80,82,84,85,87–98,100].
- Meson-meson model: [34–37,39,41,42,46,68,76,81,83,89,93,96].
- Mixing of the diquark and meson structures: [36,46,52,68,70,96].

It is seen from the Tables 10–30 that our results agree well (within the ± 50 MeV range) with the following results:

- For the $cc\bar{c}\bar{c}$ tetraquark:
 - in the diquark-antidiquark picture: [43,53,67,72,75] (all predictions); [65,84,88] (ground states only); [45,55,56,64] (1P); [63] (2S); [80,95] (3S); [35] (1S, 3S); [74] (2S, 3S); [39] (1P, 1D).
 - in the other models: [35,37–39,41,42,47,72] (all predictions); [34,83] (ground states only); [81] (2P); [70] (3S).
- For the $cb\bar{c}\bar{b}$ tetraquark:
 - in the diquark-antidiquark picture: $A\bar{A}$, $\frac{1}{\sqrt{2}}(A\bar{S} \pm S\bar{A})$, $S\bar{S}$ – [41,42,60,90] (all predictions).
 - in other models: $A\bar{A}$ – [41,42,76] (all predictions); $\frac{1}{\sqrt{2}}(A\bar{S} \pm S\bar{A})$, $S\bar{S}$ – [41,42] (all predictions).

- For the $bb\bar{b}\bar{b}$ tetraquark:
 - in the diquark-antidiquark picture: [35,40,45,60,69,90,95] (all predictions); [63] (ground states only); [66] (2S); [74] (2S, 3S).
 - in other models: [35,37,38,68] (all predictions); [39] (ground states only); [70] (3S).

A number of other conclusions can be drawn from this data:

- Predictions of Refs. [41,42] are in full agreement with our results for the $cb\bar{c}\bar{b}$ tetraquark;
- Predictions of Refs. [60,90] give good agreement for the $cb\bar{c}\bar{b}$ and $bb\bar{b}\bar{b}$ tetraquarks, but do not agree at all for the $cc\bar{c}\bar{c}$ tetraquark;
- Predictions of Refs. [35,45,63,74,95] give partial agreement for the $cc\bar{c}\bar{c}$ and $bb\bar{b}\bar{b}$ tetraquarks in the diquark-antidiquark picture;
- Predictions of Refs. [35,37–39,70] give partial agreement for the $cc\bar{c}\bar{c}$ and $bb\bar{b}\bar{b}$ tetraquarks in models other than the diquark-antidiquark.

In addition, throughout comparison of our results with those of other scientific groups shows that:

- For the $cc\bar{c}\bar{c}$ tetraquark our results are generally median: there are many results giving both heavier and lighter masses;
- For the $cb\bar{c}\bar{b}$ tetraquark masses our results exceed those of other scientific groups for all diquark spins and excitations;
- For the $bb\bar{b}\bar{b}$ tetraquark masses our results are slightly higher than those of most other scientific groups.

The generally higher values of tetraquark masses predicted in our model originate primarily from taking into account the finite size of the diquark. It results in weakening of the one-gluon exchange potential and, thus, increasing the tetraquark mass.

Note that the authors of Ref. [57] came to an unexpected conclusions. They argue that the ground state of the asymmetric tetraquark $bb\bar{c}\bar{b}$ may be stable (its ground states have been studied by us in Refs. [14,15] and were found to be significantly above the fall-apart decay thresholds), and they also expect the $cb\bar{c}\bar{b}$ tetraquark to be a narrow state in contradiction with our conclusions.

7. Conclusions

Within the framework of the relativistic quark model, we calculated masses of the ground states, radial (up to 3S) and orbital (up to 1D) excitations of the fully-charmed $cc\bar{c}\bar{c}$, doubly charmed-bottom $cb\bar{c}\bar{b}$ and fully-bottom $bb\bar{b}\bar{b}$ tetraquarks. An important feature of our calculations is the consistent account of the relativistic effects and the finite size of the diquark (as it is shown in the Sec. 3), which leads to the weakening of the one-gluon exchange potential due to the form factors of the diquark–gluon interaction.

A detailed analysis of the calculated mass spectra was carried out. We compared calculated tetraquark masses with the thresholds of the strong fall-apart decays into the meson pairs. As it is shown in Sec. 5, most of the tetraquark states lie significantly above the meson pair decay threshold. However, tetraquark states with the smallest widths and, as a result, with the most probability to be observed as narrow states have been identified. An argument is given why the excited states in general can be narrow, despite the large phase space.

It should be noted that the mass of the narrow state X(6900) recently discovered in the di- J/ψ pair production (LHCb 2020 [5], CMS 2022 [6], ATLAS 2022 [7]) agrees well with our prediction for the masses of the fully-charmed tetraquark excited (2S, 1D) states. According to the calculations, several candidates for the interpretation of this state are proposed. Candidates are also identified for all other recently discovered states such as X(6200) (ATLAS), X(6400) (LHCb), X(6600) (CMS, ATLAS), X(7200) (LHCb, ATLAS), X(7300) (CMS).

In conclusion, we note that experimental searches for fully-heavy tetraquarks are currently ongoing and should be continued. Therefore, it can be expected that new experimental candidates will appear in the near future.

Author Contributions: Authors contributed equally to the preparation of the manuscript. All authors have read and agreed to the published version of the manuscript.

Funding: The work of Elena M. Savchenko was funded in part by the Foundation for the Advancement of Theoretical Physics and Mathematics “BASIS” grant number 22-2-10-3-1.

Acknowledgments: The authors are grateful to D. Ebert for very fruitful and pleasant collaboration in developing the diquark-antidiquark model of tetraquarks. We are grateful to A.V. Berezhnoy for useful discussions.

Conflicts of Interest: The authors declare no conflict of interest.

References

- Choi, S.K. et al. Observation of a Narrow Charmoniumlike State in Exclusive $B^\pm \rightarrow K^\pm \pi^+ \pi^- J/\psi$ Decays. *Phys. Rev. Lett.* **2003**, *91*, 262001, [[hep-ex/0309032](#)]. doi:10.1103/PhysRevLett.91.262001.
- Workman, R.L. et al. Review of Particle Physics. *Prog. Theor. Exp. Phys.* **2022**, *2022*, 083C01. doi:10.1093/ptep/ptac097.
- Tornqvist, N.A. Isospin breaking of the narrow charmonium state of Belle at 3872 MeV as a deuson. *Phys. Lett. B* **2004**, *590*, 209–215, [[hep-ph/0402237](#)]. doi:10.1016/j.physletb.2004.03.077.
- Aaij, R. et al. Observation of the Resonant Character of the $Z(4430)^-$ State. *Phys. Rev. Lett.* **2014**, *112*, 222002, [[arXiv:hep-ex/1404.1903](#)]. doi:10.1103/PhysRevLett.112.222002.
- Aaij, R. et al. Observation of structure in the J/ψ -pair mass spectrum. *Sci. Bull.* **2020**, *65*, 1983–1993. doi:10.1016/j.scib.2020.08.032.
- Observation of new structures in the $J/\psi J/\psi$ mass spectrum in pp collisions at $\sqrt{s} = 13$ TeV. Technical report, CERN, Geneva, 2022.
- Observation of an excess of di-charmonium events in the four-muon final state with the ATLAS detector. Technical report, CERN, Geneva, 2022.
- Aaij, R. et al. Observation of $J/\psi p$ Resonances Consistent with Pentaquark States in $\Lambda_b^0 \rightarrow J/\psi K^- p$ Decays. *Phys. Rev. Lett.* **2015**, *115*, 072001, [[arXiv:hep-ex/1507.03414](#)]. doi:10.1103/PhysRevLett.115.072001.
- Chen, H.X.; Chen, W.; Liu, X.; Liu, Y.R.; Zhu, S.L. An updated review of the new hadron states **2022**. [[arXiv:hep-ph/2204.02649](#)]. doi:10.48550/arXiv.2204.02649.
- Aaij, R. et al. Search for beautiful tetraquarks in the $Y(1S)\mu^+\mu^-$ invariant-mass spectrum. *J. High Energy Phys.* **2018**, *2018*, 086, [[arXiv:hep-ex/1806.09707](#)]. doi:10.1007/JHEP10(2018)086.
- Khachatryan, V. et al. Observation of $Y(1S)$ pair production in proton-proton collisions at $\sqrt{s} = 8$ TeV. *J. High Energy Phys.* **2017**, *05*, 013, [[arXiv:hep-ex/1610.07095](#)]. doi:10.1007/JHEP05(2017)013.
- Sirunyan, A.M. et al. Measurement of the $Y(1S)$ pair production cross section and search for resonances decaying to $Y(1S)\mu^+\mu^-$ in proton-proton collisions at $\sqrt{s} = 13$ TeV. *Phys. Lett. B* **2020**, *808*, 135578, [[2002.06393](#)]. doi:10.1016/j.physletb.2020.135578.
- Bigi, I.; Dokshitzer, Y.; Khoze, V.; Kühn, J.; Zerwas, P. Production and decay properties of ultra-heavy quarks. *Phys. Lett. B* **1986**, *181*, 157–163. doi:10.1016/0370-2693(86)91275-x.
- Faustov, R.N.; Galkin, V.O.; Savchenko, E.M. Masses of the $QQ\bar{Q}\bar{Q}$ tetraquarks in the relativistic diquark-antidiquark picture. *Phys. Rev. D* **2020**, *102*, 114030, [[arXiv:hep-ph/2009.13237](#)]. doi:10.1103/PhysRevD.102.114030.
- Faustov, R.N.; Galkin, V.O.; Savchenko, E.M. Heavy Tetraquarks in the Relativistic Quark Model. *Universe* **2021**, *7*, 94, [[arXiv:hep-ph/2103.01763](#)]. doi:10.3390/universe7040094.
- Ebert, D.; Faustov, R.N.; Galkin, V.O. Masses of heavy baryons in the relativistic quark model. *Phys. Rev. D* **2005**, *72*, 034026, [[arXiv:hep-ph/hep-ph/0504112](#)]. doi:10.1103/PhysRevD.72.034026.
- Ebert, D.; Faustov, R.N.; Galkin, V.O. Spectroscopy and Regge trajectories of heavy baryons in the relativistic quark-diquark picture. *Phys. Rev. D* **2011**, *84*, 014025, [[arXiv:hep-ph/1105.0583](#)]. doi:10.1103/PhysRevD.84.014025.
- Logunov, A.A.; Tavkhelidze, A.N. Quasi-Optical Approach in Quantum Field Theory. *Nuovo Cim.* **1963**, *29*, 380–399. doi:10.1007/BF02750359.
- Martynenko, A.P.; Faustov, R.N. Relativistic reduced mass and quasipotential equation. *Theor. Math. Phys.* **1985**, *64*, 765–770. doi:10.1007/BF01017955.
- Galkin, V.O.; Faustov, R.N. Some properties of the solutions of a quasipotential equation. *Theor. Math. Phys.* **1990**, *85*, 1119–1123. doi:10.1007/bf01017254.
- Ebert, D.; Faustov, R.N.; Galkin, V.O.; Martynenko, A.P. Mass spectra of doubly heavy baryons in the relativistic quark model. *Phys. Rev. D* **2002**, *66*, 014008, [[hep-ph/0201217](#)]. doi:10.1103/PhysRevD.66.014008.
- Ebert, D.; Faustov, R.N.; Galkin, V.O. Masses of heavy tetraquarks in the relativistic quark model. *Phys. Lett. B* **2006**, *634*, 214–219, [[hep-ph/0512230](#)]. doi:10.1016/j.physletb.2006.01.026.
- Simonov, Y.A. Perturbation theory in the nonperturbative QCD vacuum. *Phys. Atom. Nucl.* **1995**, *58*, 107–123, [[arXiv:hep-ph/hep-ph/9311247](#)]. doi:10.48550/arXiv.HEP-PH/9311247.
- Badalian, A.M.; Veselov, A.I.; Bakker, B.L.G. Restriction on the strong coupling constant in the IR region from the 1D-1P splitting in bottomonium. *Phys. Rev. D* **2004**, *70*, 016007. doi:10.1103/PhysRevD.70.016007.
- Galkin, V.O.; Mishurov, A.Y.; Faustov, R.N. Meson masses in the relativistic quark model. *Sov. J. Nucl. Phys.* **1992**, *55*, 1207–1213.
- Ebert, D.; Faustov, R.N.; Galkin, V.O.; Lucha, W. Masses of tetraquarks with two heavy quarks in the relativistic quark model. *Phys. Rev. D* **2007**, *76*, 114015, [[0706.3853](#)]. doi:10.1103/PhysRevD.76.114015.
- Faustov, R. Magnetic Moment of the Relativistic Composite System. *Nuovo Cim. A* **1970**, *69*, 37–46. doi:10.1007/BF02728769.
- Faustov, R.N. Relativistic Wawefunction and Form Factors of the Bound System. *Annals Phys.* **1973**, *78*, 176–189. doi:10.1016/0003-4916(73)90007-9.

29. Galkin, V.O.; Faustov, R.N. Relativistic corrections to radiative decay widths of vector mesons. *Sov. J. Nucl. Phys.* **1986**, *44*, 1575–1581.
30. Galkin, V.O.; Mishurov, A.Y.; Faustov, R.N. Radiative E1 decays of quarkonium in the framework of relativistic quark model. *Sov. J. Nucl. Phys.* **1990**, *51*, 705–710.
31. Faustov, R.N.; Galkin, V.O. Heavy quark $1/m_Q$ expansion of meson weak decay form-factors in the relativistic quark model. *Z Phys. C* **1995**, *66*, 119–127. doi:10.1007/BF01496586.
32. Dong, X.K.; Baru, V.; Guo, F.K.; Hanhart, C.; Nefediev, A. Coupled-Channel Interpretation of the LHCb Double- J/ψ Spectrum and Hints of a New State Near the $J/\psi J/\psi$ Threshold. *Phys. Rev. Lett.* **2021**, *126*, 132001, [arXiv:hep-ph/2009.07795]. [Erratum: Phys.Rev.Lett. 127, 119901 (2021)], doi:10.1103/PhysRevLett.126.132001.
33. Hughes, C.; Eichten, E.; Davies, C.T.H. Searching for beauty-fully bound tetraquarks using lattice nonrelativistic QCD. *Phys. Rev. D* **2018**, *97*, 054505. doi:10.1103/PhysRevD.97.054505.
34. Ader, J.P.; Richard, J.M.; Taxil, P. Do narrow heavy multiquark states exist? *Phys. Rev. D* **1982**, *25*, 2370. doi:10.1103/PhysRevD.25.2370.
35. Jin, X.; Xue, Y.; Huang, H.; Ping, J. Full-heavy tetraquarks in constituent quark models. *Eur. Phys. J. C* **2020**, *80*, 1083, [arXiv:hep-ph/2006.13745]. doi:10.1140/epjc/s10052-020-08650-z.
36. Chen, X. Fully-charm tetraquarks: $cc\bar{c}\bar{c}$ **2020**. [arXiv:hep-ph/2001.06755]. doi:10.48550/arXiv.2001.06755.
37. Albuquerque, R.M.; Narison, S.; Rabemananjara, A.; Rabetiariivony, D.; Randriamanatrika, G. Doubly-hidden scalar heavy molecules and tetraquarks states from QCD at NLO. *Phys. Rev. D* **2020**, *102*, 094001. doi:10.1103/PhysRevD.102.094001.
38. Albuquerque, R.M.; Narison, S.; Rabetiariivony, D.; Randriamanatrika, G. Doubly hidden 0^{++} molecules and tetraquarks states from QCD at NLO. *Nucl. Part. Phys. Proc.* **2021**, *312-317*, 15289, [arXiv:hep-ph/2102.08776]. doi:10.1016/j.nuclphysbps.2021.05.031.
39. Wu, R.H.; Zuo, Y.S.; Wang, C.Y.; Meng, C.; Ma, Y.Q.; Chao, K.T. NLO results with operator mixing for fully heavy tetraquarks in QCD sum rules **2022**. [arXiv:hep-ph/2201.11714]. doi:10.48550/arXiv.2201.11714.
40. Deng, C.; Chen, H.; Ping, J. Towards the understanding of fully-heavy tetraquark states from various models. *Phys. Rev. D* **2021**, *103*, 014001. doi:10.1103/PhysRevD.103.014001.
41. Yang, G.; Ping, J.; Segovia, J. Exotic resonances of fully-heavy tetraquarks in a lattice-QCD inspired quark model. *Phys. Rev. D* **2021**, *104*, 014006. doi:10.1103/PhysRevD.104.014006.
42. Yang, G.; Ping, J.; He, L.; Wang, Q. Potential model prediction of fully-heavy tetraquarks $QQ\bar{Q}\bar{Q}$ ($Q = c, b$) **2021**. [arXiv:hep-ph/2006.13756]. doi:10.48550/arXiv.2006.13756.
43. Anwar, M.N.; Ferretti, J.; Guo, F.K.; Santopinto, E.; Zou, B.S. Spectroscopy and decays of the fully-heavy tetraquarks. *Eur. Phys. J. C* **2018**, *78*, 647, [arXiv:hep-ph/1710.02540]. doi:10.1140/epjc/s10052-018-6073-9.
44. Asadi, Z.; Boroun, G.R. Masses of fully heavy tetraquark states from a four-quark static potential model. *Phys. Rev. D* **2022**, *105*, 014006. doi:10.1103/PhysRevD.105.014006.
45. Liu, M.S.; Liu, F.X.; Zhong, X.H.; Zhao, Q. Full-heavy tetraquark states and their evidences in the LHCb $di - J/\psi$ spectrum **2020**. [arXiv:hep-ph/2006.11952]. doi:10.48550/arXiv.2006.11952.
46. Chen, X. Analysis of hidden-bottom $bb\bar{b}\bar{b}$ states. *Eur. Phys. J. A* **2019**, *55*, 106, [arXiv:hep-ph/1902.00008]. doi:10.1140/epja/i2019-12807-2.
47. Iwasaki, Y. A Possible Model for New Resonances – Exotics and Hidden Charm. *Prog. Theor. Phys.* **1975**, *54*, 492. doi:10.1143/PTP.54.492.
48. Lloyd, R.J.; Vary, J.P. All-charm tetraquarks. *Phys. Rev. D* **2004**, *70*, 014009. doi:10.1103/PhysRevD.70.014009.
49. Barnea, N.; Vijande, J.; Valcarce, A. Four-quark spectroscopy within the hyperspherical formalism. *Phys. Rev. D* **2006**, *73*, 054004. doi:10.1103/PhysRevD.73.054004.
50. Berezhnoy, A.V.; Likhoded, A.K.; Luchinsky, A.V.; Novoselov, A.A. Production of J/ψ -meson pairs and $4c$ tetraquark at the LHC. *Phys. Rev. D* **2011**, *84*, 094023. doi:10.1103/PhysRevD.84.094023.
51. Berezhnoy, A.V.; Luchinsky, A.V.; Novoselov, A.A. Heavy tetraquarks production at the LHC. *Phys. Rev. D* **2012**, *86*, 034004. doi:10.1103/PhysRevD.86.034004.
52. Heupel, W.; Eichmann, G.; Fischer, C.S. Tetraquark bound states in a Bethe–Salpeter approach. *Phys. Lett. B* **2012**, *718*, 545–549. doi:10.1016/j.physletb.2012.11.009.
53. Karliner, M.; Nussinov, S.; Rosner, J.L. $QQ\bar{Q}\bar{Q}$ states: Masses, production, and decays. *Phys. Rev. D* **2017**, *95*, 034011, [arXiv:hep-ph/1611.00348]. doi:10.1103/PhysRevD.95.034011.
54. Wang, Z.G. Analysis of the $QQ\bar{Q}\bar{Q}$ tetraquark states with QCD sum rules. *Eur. Phys. J. C* **2017**, *77*, 432, [arXiv:hep-ph/1701.04285]. doi:10.1140/epjc/s10052-017-4997-0.
55. Chen, W.; Chen, H.X.; Liu, X.; Steele, T.G.; Zhu, S.L. Hunting for exotic doubly hidden-charm/bottom tetraquark states. *Phys. Lett. B* **2017**, *773*, 247–251. doi:10.1016/j.physletb.2017.08.034.
56. Chen, W.; Chen, H.X.; Liu, X.; Steele, T.G.; Zhu, S.L. Doubly hidden-charm/bottom $QQ\bar{Q}\bar{Q}$ tetraquark states. *EPJ Web Conf.* **2018**, *182*, 02028, [arXiv:hep-ph/1803.02522]. doi:10.1051/epjconf/201818202028.
57. Wu, J.; Liu, Y.R.; Chen, K.; Liu, X.; Zhu, S.L. Heavy-flavored tetraquark states with the $QQ\bar{Q}\bar{Q}$ configuration. *Phys. Rev. D* **2018**, *97*, 094015. doi:10.1103/PhysRevD.97.094015.
58. Debastiani, V.R.; Navarra, F.S. Spectroscopy of the All-Charm Tetraquark. Proceedings of XVII International Conference on Hadron Spectroscopy and Structure — PoS(Hadron2017), 2018, Vol. 310, p. 238, [arXiv:hep-ph/1711.11495]. doi:10.22323/1.310.0238.

59. Debastiani, V.R.; Navarra, F.S. A non-relativistic model for the $[cc][\bar{c}\bar{c}]$ tetraquark. *Chinese Phys. C* **2019**, *43*, 013105. doi:10.1088/1674-1137/43/1/013105.
60. Liu, M.S.; Lü, Q.F.; Zhong, X.H.; Zhao, Q. All-heavy tetraquarks. *Phys. Rev. D* **2019**, *100*, 016006. doi:10.1103/PhysRevD.100.016006.
61. Bai, Y.; Lu, S.; Osborne, J. Beauty-full tetraquarks. *Phys. Lett. B* **2019**, *798*, 134930. doi:https://doi.org/10.1016/j.physletb.2019.134930.
62. Wang, Z.G.; Di, Z.Y. Analysis of the Vector and Axialvector $QQ\bar{Q}\bar{Q}$ Tetraquark States with QCD Sum Rules. *Acta Phys. Polon. B* **2019**, *50*, 1335, [arXiv:hep-ph/1807.08520]. doi:10.5506/APhysPolB.50.1335.
63. Wang, G.J.; Meng, L.; Zhu, S.L. Spectrum of the fully-heavy tetraquark state $QQ\bar{Q}'\bar{Q}'$. *Phys. Rev. D* **2019**, *100*, 096013. doi:10.1103/PhysRevD.100.096013.
64. Bedolla, M.A.; Ferretti, J.; Roberts, C.D.; Santopinto, E. Spectrum of fully-heavy tetraquarks from a diquark+antidiquark perspective. *Eur. Phys. J. C* **2020**, *80*, 1004, [arXiv:hep-ph/1911.00960]. doi:10.1140/epjc/s10052-020-08579-3.
65. Karliner, M.; Rosner, J.L. Interpretation of structure in the $di - J/\psi$ spectrum. *Phys. Rev. D* **2020**, *102*, 114039. doi:10.1103/PhysRevD.102.114039.
66. Lü, Q.F.; Chen, D.Y.; Dong, Y.B. Masses of fully heavy tetraquarks $QQ\bar{Q}\bar{Q}$ in an extended relativized quark model. *Eur. Phys. J. C* **2020**, *80*, 871, [arXiv:hep-ph/2006.14445]. doi:10.1140/epjc/s10052-020-08454-1.
67. Lundhammar, P.; Ohlsson, T. Nonrelativistic model of tetraquarks and predictions for their masses from fits to charmed and bottom meson data. *Phys. Rev. D* **2020**, *102*, 054018, [arXiv:hep-ph/2006.09393]. doi:10.1103/PhysRevD.102.054018.
68. Yang, G.; Ping, J.; Segovia, J. Tetra- and Penta-Quark Structures in the Constituent Quark Model. *Symmetry* **2020**, *12*, 1869, [arXiv:hep-ph/2009.00238]. doi:10.3390/sym12111869.
69. Gordillo, M.C.; De Soto, F.; Segovia, J. Diffusion Monte Carlo calculations of fully-heavy multi-quark bound states. *Phys. Rev. D* **2020**, *102*, 114007, [arXiv:hep-ph/2009.11889]. doi:10.1103/PhysRevD.102.114007.
70. Zhao, J.; Shi, S.; Zhuang, P. Fully-heavy tetraquarks in a strongly interacting medium. *Phys. Rev. D* **2020**, *102*, 114001. doi:10.1103/PhysRevD.102.114001.
71. Zhang, J.R. 0^+ fully-charmed tetraquark states. *Phys. Rev. D* **2021**, *103*, 014018. doi:10.1103/PhysRevD.103.014018.
72. Obikhod, T.V. Application of the triangulated category to the explanation of fully-charm tetraquark mass. 2021, [arXiv:hep-ph/2103.08449]. doi:10.48550/arXiv.2103.08449.
73. Wang, Z.G. Revisit the tetraquark candidates in the $J/\psi/\psi$ mass spectrum. *Int. J. Mod. Phys. A* **2021**, *36*, 2150014, [arXiv:hep-ph/2009.05371]. doi:10.1142/S0217751X21500147.
74. Li, Q.; Chang, C.H.; Wang, G.L.; Wang, T. Mass spectra and wave functions of $T_{QQ\bar{Q}\bar{Q}}$ tetraquarks. *Phys. Rev. D* **2021**, *104*, 014018. doi:10.1103/PhysRevD.104.014018.
75. Nefediev, A.V. $X(6200)$ as a compact tetraquark in the QCD string model. *Eur. Phys. J. C* **2021**, *81*, 692, [arXiv:hep-ph/2107.14182]. doi:10.1140/epjc/s10052-021-09511-z.
76. Yang, B.C.; Tang, L.; Qiao, C.F. Scalar fully-heavy tetraquark states $QQ'\bar{Q}\bar{Q}'$ in QCD sum rules. *Eur. Phys. J. C* **2021**, *81*, 324, [arXiv:hep-ph/2012.04463]. doi:10.1140/epjc/s10052-021-09096-7.
77. Weng, X.Z.; Chen, X.L.; Deng, W.Z.; Zhu, S.L. Systematics of fully heavy tetraquarks. *Phys. Rev. D* **2021**, *103*, 034001. doi:10.1103/PhysRevD.103.034001.
78. Tiwari, R.; Rathaud, D.P.; Rai, A.K. Spectroscopy of all charm tetraquark states. *Indian J. Phys.* **2022**, [arXiv:hep-ph/2108.04017]. doi:10.1007/s12648-022-02427-8.
79. Wang, G.J.; Meng, L.; Oka, M.; Zhu, S.L. Higher fully charmed tetraquarks: Radial excitations and P -wave states. *Phys. Rev. D* **2021**, *104*, 036016. doi:10.1103/PhysRevD.104.036016.
80. Zhao, Z.; Xu, K.; Kaewnsnod, A.; Liu, X.; Limphirat, A.; Yan, Y. Study of charmoniumlike and fully-charm tetraquark spectroscopy. *Phys. Rev. D* **2021**, *103*, 116027. doi:10.1103/PhysRevD.103.116027.
81. Lesteiro-Tejeda, J.A.; Ramírez-Zaldívar, D.A.; Gracia-Trápaga, C.E.; Guzmán-Martínez, F. Spectroscopy of the tetraquark $c\bar{c} - c\bar{c}$ in a non-relativistic approach using a phenomenological QCD model **2021**. [arXiv:hep-ph/2101.03192]. doi:10.48550/arXiv.2101.03192.
82. Mutuk, H. Nonrelativistic treatment of fully-heavy tetraquarks as diquark-antidiquark states. *Eur. Phys. J. C* **2021**, *81*, 367, [arXiv:hep-ph/2104.11823]. doi:10.1140/epjc/s10052-021-09176-8.
83. Wang, Q.N.; Yang, Z.Y.; Chen, W. Exotic fully heavy $QQ\bar{Q}\bar{Q}$ tetraquark states in $8_{[Q\bar{Q}]} \otimes 8_{[Q\bar{Q}]}$ color configuration. *Phys. Rev. D* **2021**, *104*, 114037. doi:10.1103/PhysRevD.104.114037.
84. Ke, H.W.; Han, X.; Liu, X.H.; Shi, Y.L. Tetraquark state $X(6900)$ and the interaction between diquark and antidiquark. *Eur. Phys. J. C* **2021**, *81*, 427, [arXiv:hep-ph/2103.13140]. doi:10.1140/epjc/s10052-021-09229-y.
85. Zhu, R. Fully-heavy tetraquark spectra and production at hadron colliders. *Nucl. Phys. B* **2021**, *966*, 115393. doi:https://doi.org/10.1016/j.nucphysb.2021.115393.
86. Kuang, Z.; Serafin, K.; Zhao, X.; Vary, J.P. All-charm tetraquark in front form dynamics. *Phys. Rev. D* **2022**, *105*, 094028, [arXiv:hep-ph/2201.06428]. doi:10.1103/PhysRevD.105.094028.
87. Majarshin, A.J.; Luo, Y.A.; Pan, F.; Segovia, J. Bosonic algebraic approach applied to the $[QQ][\bar{Q}\bar{Q}]$ tetraquarks. *Phys. Rev. D* **2022**, *105*, 054024, [arXiv:hep-ph/2106.01179]. doi:10.1103/PhysRevD.105.054024.
88. Wang, Z.G. Analysis of the $X(6600)$, $X(6900)$, $X(7300)$ and related tetraquark states with the QCD sum rules **2022**. [arXiv:hep-ph/2207.08059]. doi:10.48550/arXiv.2207.08059.
89. Wang, G.J.; Meng, Q.; Oka, M. The S-wave fully-charmed tetraquark resonant states **2022**. [arXiv:hep-ph/2208.07292]. doi:10.48550/arXiv.2208.07292.
90. An, H.T.; Luo, S.Q.; Liu, Z.W.; Liu, X. Systematic search of fully heavy tetraquark states **2022**. [arXiv:hep-ph/2208.03899]. doi:10.48550/arXiv.2208.03899.

-
91. Zhuang, Z.; Zhang, Y.; Ma, Y.; Wang, Q. Lineshape of the compact fully heavy tetraquark. *Phys. Rev. D* **2022**, *105*, 054026. doi:10.1103/PhysRevD.105.054026.
 92. Chao, K.T. The $(cc) - (\bar{c}\bar{c})$ (Diquark - Antidiquark) States in e^+e^- Annihilation. *Z. Phys. C* **1981**, *7*, 317. doi:10.1007/BF01431564.
 93. Chiu, T.W.; Hsieh, T.H. $Y(4260)$ on the lattice. *Phys. Rev. D* **2006**, *73*, 094510, [[hep-lat/0512029](#)]. doi:10.1103/PhysRevD.73.094510.
 94. Wang, Z.G. Tetraquark candidates in LHCb's $di - J/\psi$ mass spectrum. *Chinese Phys. C* **2020**, *44*, 113106. doi:10.1088/1674-1137/abb080.
 95. Liu, F.X.; Liu, M.S.; Zhong, X.H.; Zhao, Q. Higher mass spectra of the fully-charmed and fully-bottom tetraquarks. *Phys. Rev. D* **2021**, *104*, 116029. doi:10.1103/PhysRevD.104.116029.
 96. Chen, X. Fully-heavy tetraquarks: $bb\bar{c}\bar{c}$ and $bc\bar{b}\bar{c}$. *Phys. Rev. D* **2019**, *100*, 094009, [[arXiv:hep-ph/1908.08811](#)]. doi:10.1103/PhysRevD.100.094009.
 97. Yang, Z.Y.; Wang, Q.N.; Chen, W.; Chen, H.X. Investigation of the stability for fully-heavy $bc\bar{b}\bar{c}$ tetraquark states. *Phys. Rev. D* **2021**, *104*, 014003. doi:10.1103/PhysRevD.104.014003.
 98. Esposito, A.; Polosa, A.D. A $bb\bar{b}\bar{b}$ di-bottomonium at the LHC? *Eur. Phys. J. C* **2018**, *78*, 782, [[arXiv:hep-ph/1807.06040](#)]. doi:10.1140/epjc/s10052-018-6269-z.
 99. Vogt, R.; Angerami, A. Bottom tetraquark production at RHIC? *Phys. Rev. D* **2021**, *104*, 094025. doi:10.1103/PhysRevD.104.094025.
 100. Tiwari, R.; Rathaud, D.P.; Rai, A.K. Mass-spectroscopy of $[bb][\bar{b}\bar{b}]$ and $[bq][\bar{b}\bar{q}]$ tetraquark states in a diquark-antidiquark formalism. *Eur. Phys. J. A* **2021**, *57*. doi:10.1140/epja/s10050-021-00601-w.